The Astrophysical Journal Supplement Series, 151:271–297, 2004 April
© 2004. The American Astronomical Society. All rights reserved. Printed in U.S.A.

THE MILLENNIUM ARECIBO 21 CENTIMETER ABSORPTION-LINE SURVEY. III. TECHNIQUES FOR SPECTRAL POLARIZATION AND RESULTS FOR STOKES *V*

Carl Heiles
Astronomy Department, University of California, Berkeley, CA 94720-3411; cheiles@astron.berkeley.edu

and

T. H. Troland
Department of Physics and Astronomy, University of Kentucky, Lexington, KY 40506; troland@pa.uky.edu
Received 2003 October 1; accepted 2003 December 2

ABSTRACT

We outline the theory and practice of measuring the four Stokes parameters of spectral lines in emission/absorption observations. We apply these concepts to our Arecibo H I absorption line data and present the results. We include a detailed discussion of instrumental effects arising from polarized beam structure and its interaction with the spatially extended emission line structure. At Arecibo, linear polarization [Stokes (Q, U)] has much larger instrumental effects than circular (Stokes V). We show how to reduce the instrumental contributions to V and to evaluate upper limits to its remaining instrumental errors by using the (Q, U) results. These efforts work well for opacity spectra but not for emission spectra. Arecibo's large central blockage exacerbates these effects, particularly for emission profiles, and other telescopes with weaker sidelobes are not as susceptible. We present graphical results for 41 sources; we analyze these absorption spectra in terms of Gaussian components, which number 136, and present physical parameters including magnetic field for each.

Subject headings: polarization — radio lines: ISM — surveys

On-line material: additional figures, machine-readable table

1. INTRODUCTION

In 1999 February we used the Arecibo[1] telescope to begin a series of Zeeman-splitting measurements of the 21 cm line in absorption against continuum radio sources. Heiles & Troland (2003a, 2003b, hereafter Paper I and Paper II) reported on a by-product of this survey, namely the Stokes I data from which spin temperatures and other information were derived. The present paper focuses on the technical aspects of processing the polarized spectral data and evaluating the instrumental errors. We also present the derived magnetic fields for 41 sources, which have 136 Gaussian components.

There has been much discussion of H I Zeeman splitting measurements because the polarized sidelobes, interacting with the angular structure of the H I emission, can produce instrumental effects. Even in the emission-absorption measurements presented in this paper, these effects can in principle be serious. Therefore, we discuss these effects in considerable detail. The bottom line is that instrumental effects are evaluated for each source independently and, generally, are negligible for the opacity spectra. However, for the expected emission spectra they are not negligible.

Section 2 outlines the basic theoretical concepts involving Stokes parameters and emission/absorption lines. Section 3 discusses the least-squares fitting process required to extract the expected emission profile and the absorption spectrum by combining calibrated on- and off-source data. Section 4 discusses the physical reasons for and contributors to instrumental effects that arise from polarized beam structure.

The next three sections deal with instrumental contributions to the *opacity* spectra. We begin by treating Stokes V in § 5, discussing the empirical least-squares evaluation and elimination of the two most basic instrumental effects, namely the trigonometric dependences on parallactic angle PA and 2PA (squintlike and squashlike dependences, respectively). We use the terms "squintlike" and "squashlike" for these empirically determined dependencies because they include contributions from far-out sidelobes; in contrast, we use the terms "squint" and "squash" (sometimes preceded by the clarifier "true") for the contributions from only the primary beam and first sidelobe.[2] We then do the same in § 6 for the linearly polarized Stokes parameters (Q, U). We reach the important conclusion that instrumental effects in linear polarization are about 10 times larger than in circular. This allows us to make an independent estimate of instrumental effects for V using (Q, U), as we discuss explicitly in § 7.

Our final discussion of instrumental effects (§ 8) addresses the reliability of Zeeman splitting results for *emission* profiles. Here we independently evaluate "true" squint and squash and also the squintlike and squashlike contributions. The difference between these is the contributions from the far-out sidelobes. The far-out sidelobe contribution is large for the Arecibo telescope. This makes the instrumental effects quite serious for emission profiles. Accordingly, we do not discuss the Zeeman splitting results for the emission profiles.

[1] The Arecibo Observatory is part of the National Astronomy and Ionosphere Center, which is operated by Cornell University under a cooperative agreement with the National Science Foundation.

[2] The terms squint and squash normally refer to only to the main beam, not including the first sidelobe.

Finally, § 9 presents the profiles for all sources and a tabular list of the results for the Gaussian components. We select a good sample for statistical analyses, successfully compare with previous literature, and point out yet another source of uncertainty in the derived magnetic fields.

2. STOKES PARAMETERS OF SPECTRAL LINES IN EMISSION/ABSORPTION

2.1. *The ON and OFF Spectra*

Consider a particular polarization, which we designate by the subscript p. For the two circulars we have $p = \mathrm{LCP}$ or $p = \mathrm{RCP}$, while for the linears we have $p =$ position angle. In the presence of a continuum source that provides antenna temperature $T_{\mathrm{src},\,p}$, the on-source antenna temperature is

$$T_{\mathrm{src},\,p}(\nu) = T_{\mathrm{exp},\,p}(\nu) + T_{\mathrm{src},\,p}e^{-\tau_p(\nu)}, \tag{1}$$

where $T_{\mathrm{exp},\,p}(\nu)$ is the "expected profile," which is the emission that would be observed in the absence of the source, and $\tau_p(\nu)$ is the 21 cm line opacity, which depends on polarization; both of these are functions of frequency because of the spectral line. The appended symbol (ν) indicates frequency-dependent quantities within the profile; unappended temperatures are continuum.

We form Stokes parameters for the on-source antenna temperature from arithmetic combinations of orthogonal polarizations (p, $p_\perp$). We designate the Stokes parameters I_{src}, Q_{src}, U_{src}, and V_{src} with the general symbol $S_{\mathrm{src},\,i}$, with $i = 0 \rightarrow 3$, respectively; the subscript "src" designates on-source "antenna" Stokes parameters, derived from on-source antenna temperatures. This gives for Stokes I_{src}

$$S_{\mathrm{src},0}(\nu) = [T_{\mathrm{exp},\,p}(\nu) + T_{\mathrm{exp},\,p_\perp}(\nu)] + [T_{\mathrm{src},\,p}e^{-\tau_p(\nu)} + T_{\mathrm{src},\,p_\perp}e^{-\tau_{p\perp}(\nu)}], \tag{2a}$$

and for Stokes $(Q_{\mathrm{src}}, U_{\mathrm{src}}, V_{\mathrm{src}})$

$$S_{\mathrm{src},i}(\nu) = [T_{\mathrm{exp},\,p}(\nu) - T_{\mathrm{exp},\,p_\perp}(\nu)] + [T_{\mathrm{src},\,p}e^{-\tau_p(\nu)} - T_{\mathrm{src},\,p_\perp}e^{-\tau_{p\perp}(\nu)}], \quad (i = 1 \rightarrow 3). \tag{2b}$$

Here and below, (i) implies $i = 1 \rightarrow 3$ unless otherwise noted, and p must correspond correctly with i.

We define

$$\tau_0(\nu) \equiv \frac{\tau_p(\nu) + \tau_{p_\perp}(\nu)}{2}, \tag{3a}$$

and we assume that the spectral line exhibits small polarization, i.e.,

$$\tau_i(\nu) \equiv \tau_p(\nu) - \tau_{p_\perp}(\nu) \ll 1, \tag{3b}$$

where again p must correspond correctly with i. Then we expand equations (2a) and (2b) and retain only the lowest order terms in τ_i, which are zeroth order for equation (2a) and first order for equation (2b). This gives

$$S_{\mathrm{src},0}(\nu) = [T_{\mathrm{exp},\,p}(\nu) + T_{\mathrm{exp},\,p_\perp}(\nu)] + [T_{\mathrm{src},\,p} + T_{\mathrm{src},\,p_\perp}]e^{-\tau_0(\nu)}, \tag{4a}$$

$$S_{\mathrm{src},i}(\nu) = [T_{\mathrm{exp},\,p}(\nu) - T_{\mathrm{exp},\,p_\perp}(\nu)] - \tau_i(\nu)\frac{[T_{\mathrm{src},\,p} + T_{\mathrm{src},\,p_\perp}]}{2}e^{-\tau_0(\nu)} + [T_{\mathrm{src},\,p} - T_{\mathrm{src},\,p_\perp}]e^{-\tau_0(\nu)}. \tag{4b}$$

It is clearer to write the above expressing the temperature sums and differences in terms of their Stokes parameters, which are the appropriate sums and differences of antenna temperatures:

$$S_{\mathrm{src},0}(\nu) = S_{\mathrm{exp},0}(\nu) + S_{\mathrm{src},0}e^{-\tau_0(\nu)}, \tag{5a}$$

$$S_{\mathrm{src},\,i}(\nu) = S_{\mathrm{exp},\,i}(\nu) - \tau_i(\nu)\frac{S_{\mathrm{src},0}}{2}e^{-\tau_0(\nu)} + S_{\mathrm{src},i}e^{-\tau_0(\nu)}. \tag{5b}$$

Again, quantities subscripted with "exp," like $S_{\mathrm{exp},\,i}(\nu)$, are the frequency-dependent expected profile, i.e., what is expected to be observed at the source position if its continuum flux were zero; quantities subscripted with "src," like $S_{\mathrm{src},0}$, are frequency-independent properties of the continuum source.

Equation (5b) for the polarized Stokes parameters S_i consists of three terms:

1. The first term is the polarization of the expected emission profile.
2. The second term represents the polarized portion of the optical depth $\tau_i(\nu)$ multiplying the attenuated Stokes I_{src} (or $S_{\mathrm{src},0}$) antenna temperature of the continuum source. For Zeeman splitting, this is the quantity of interest!
3. The third term represents the ordinary line opacity operating on the polarized Stokes Q, U, V (or S_i) antenna temperature of the continuum source.

2.2. *The ON-OFF Spectra*

For Stokes I, consider equation (5a) and assume, for the moment, that the spatial derivatives of $S_{\mathrm{exp},0}(\nu)$ are zero. Then the two unknowns $S_{\mathrm{exp},0}(\nu)$ and $e^{-\tau_0(\nu)}$ are easily separated observationally by taking on-source and off-source measurements, for which $S_{\mathrm{src},0}$ changes from zero to the full source intensity. More generally the spatial derivatives are nonzero; moreover, Arecibo has significant sidelobes and we can never go completely off the source. We account for these and other details by writing more complicated versions of equation (5a) and subjecting them to least-squares analyses. This is discussed in detail in § 2 of Paper I.

Now consider the polarized Stokes parameters in equation (5b) and assume that the spatial derivatives of their expected emission profiles are zero. Then the combination of the second and third terms is easily obtained by subtracting the on-source and off-source measurements (ON–OFF). Below, as we did for I, we will account for details using least-squares fits to more complicated equations. The third term in equation (5b) is of little intrinsic interest because it reveals no new information: it is simply the line opacity operating on the polarized flux. This term is often large for Stokes Q and U because radio continuum sources often exhibit significant linear polarization.

In contrast, the second term is of vital importance. In circular polarization it is nonzero because of Zeeman splitting. In linear polarization it reveals a correlation between the spatial structures of the H I and the radio source Stokes parameters. Specifically, the more highly polarized parts of the source produce larger fractional contributions to the polarized opacity profile. Unfortunately, instrumental effects also contribute to the second term; we discuss these in § 4.

2.3. *The Particular Case of Zeeman Splitting*

Zeeman splitting is characterized by a frequency difference between the two circular polarizations, so are concerned with the subscript $i = 3$. From now on we will write the subscripts with the conventional notation (Q, U, V) instead of (1, 2, 3). We have

$$\tau_V(\nu) = \frac{d\tau_0(\nu)}{d\nu}\delta\nu_Z. \tag{6}$$

As is well known, for the 21 cm line $\delta\nu_Z = 2.8B_{\|}$ Hz, where $B_{\|}$ is the line-of-sight field strength in μG. To focus on the opacity spectrum, we consider only the source terms in equations (5a)–(5b) [i.e., we set $S_{\mathrm{exp},0}(\nu) = 0$] and we assume no continuum circular polarization (i.e., we set $V_{\mathrm{src}} = 0$). Writing the usual I for S_0 and V for S_3, we have

$$I_{\mathrm{src}}(\nu) = I_{\mathrm{src}}e^{-\tau_0(\nu)}, \tag{7a}$$

$$V_{\mathrm{src}}(\nu) = -\frac{I_{\mathrm{src}}}{2}e^{-\tau_0(\nu)}\tau_V(\nu), \tag{7b}$$

or, in the most observationally relevant form,

$$V_{\mathrm{src}}(\nu) = \frac{d[I_{\mathrm{src}}(\nu)/2]}{d\nu}\delta\nu_Z. \tag{8}$$

This is exactly the same equation that applies to the optically thin emission case.

We recount this simple derivation to elucidate any possible confusion about the role of Stokes I opacity in deriving $\delta\nu_Z$. This opacity weakens the V spectrum; in particular, the effect of the opacity difference $\tau_V(\nu)$ is weakened by the factor $\exp[-\tau_0(\nu)]$, and one might have expected this weakening to reduce the derived value of $\delta\nu_Z$. This derivation shows that using equation (8) provides the correct values of $\delta\nu_Z$ under any circumstances, emission or absorption.

3. EXTRACTING POLARIZED PROFILES FROM CALIBRATED SPECTRAL DATA

3.1. *Stokes I*

Paper I discussed our observing technique and the least-squares fit for the Stokes I expected profile, its spatial derivatives, and the opacity profile. We observed a series of N "patterns," denoted by the subscript n. Each pattern consists of a series of J measurements (subscript j), one being on-source and the others being off-source displaced in different directions. This allows us to determine spatial derivatives, which was important for the analysis of the Stokes I profiles done in Paper II. Here we are concerned with the polarized Stokes parameters, which are themselves detectable only with low signal/noise and for which the spatial derivatives are expected to be undetectable. Therefore, to begin our discussion we rewrite equation (8) in Paper I without the spatial derivative terms, obtaining a slight generalization of equation (1) above:

$$T_{\mathrm{ant},n,j}(\nu) = [T_{\mathrm{exp}}(\nu)] + [e^{-\tau(\nu)}]T_{\mathrm{ant},n,j}. \tag{9}$$

The quantity $T_{\mathrm{ant},n,j}$, without the appended symbol (ν), is the excess continuum antenna temperature over cold sky, which is usually nonzero even for off-source measurements because (1) the telescope sidelobes respond to the source, (2) the off position can lie within the primary beam, and (3) diffuse continuum emission that happens to lie in the source direction also contributes. $T_{\mathrm{ant},n,j}(\nu)$ includes the effects of the H I line, while $T_{\mathrm{ant},n,j}$ does not—it is only the continuum contribution. $T_{\mathrm{ant},n,j}(\nu)$ is the antenna temperature, i.e., the input to the receiver.

This equation applies to antenna temperatures measured in a particular polarization. Therefore, it also applies to sums and differences of antenna temperatures in orthogonal polarizations, i.e., the Stokes parameters. For Stokes I the equation barely changes. However, the polarized Stokes parameters are slightly more involved.

3.2. *Stokes V*

First we treat the simpler case of Stokes V. When we form V by subtracting RCP from LCP, the left-hand side of equation (9) becomes the measured value $V_{\mathrm{ant},n,j}(\nu)$. In general, both the source and $\tau(\nu)$ are polarized, so the equation becomes

$$V_{\mathrm{ant},n,j}(\nu) - V_{\mathrm{ant},n,j}e^{-\tau_0(\nu)} = [V_{\mathrm{exp}}(\nu)] - \left[\frac{\tau_V(\nu)e^{-\tau_0(\nu)}}{2}\right] I_{\mathrm{ant},n,j} + [\Delta V_{n,j}(\nu)], \tag{10a}$$

where, as in equation (5b), we retain only first-order terms. Also, we have added an instrumental contribution $[\Delta V_{n,j}(\nu)]$, which we discuss below. Again, the square brackets indicate quantities to be solved for by least squares. In a least-squares analysis we need on one side of the equation all of the unknowns, and none of the knowns, which is why we transferred the quantity $V_{\mathrm{ant},n,j}e^{-\tau_0(\nu)}$ to the left-hand side; both factors are known reasonably accurately from the observations. To make the equations more concise, which is convenient for later discussion, we make two definitions. First, we define the quantity

$$[\tau'_V(\nu)] \equiv -\left[\frac{\tau_V(\nu)e^{-\tau_0(\nu)}}{2}\right], \tag{10b}$$

which is the fractional circular polarization of the source's absorbed flux ($V(\nu)/I_{\mathrm{src}}$ in eq. [7b]), useful because it is proportional to the frequency derivative of $I(\nu)$. Second, we define $V'_{\mathrm{sky},n,j}(\nu)$ to be the first two terms on the right-hand side of equation (10a), i.e.,

$$[V'_{\mathrm{sky},n,j}(\nu)] = [V_{\mathrm{exp}}(\nu)] + [\tau'_V(\nu)]I_{\mathrm{ant},n,j}. \tag{10c}$$

so that equation (10a) becomes

$$V_{\mathrm{ant},n,j}(\nu) - V_{\mathrm{ant},n,j}e^{-\tau_0(\nu)} = [[V'_{\mathrm{sky},n,j}(\nu)]] + [\Delta V_{n,j}(\nu)], \tag{10d}$$

where the double brackets around $[[V'_{\mathrm{sky},n,j}(\nu)]]$ serve as a reminder that this term contains more than one unknown quantity. The left-hand side contains the measured quantities: $V_{\mathrm{ant},n,j}(\nu)$ is the channel-by-channel V spectrum, while $V_{\mathrm{ant},n,j}$ (no ν dependence) is the continuum value, obtained from the off-line channels. Similarly, $I_{\mathrm{ant},n,j}$ on the right-hand side is the Stokes I continuum value, also from the off-line channels.

For each spectral independently, the quantities in square brackets are straightforwardly solved by least squares, except for the instrumental contributions $[\Delta V_{n,j}(\nu)]$ for which the word "straightforwardly" does not necessarily apply. We either ignore this contribution and estimate its magnitude, as discussed in § 8.2, or assume a functional dependence on parallactic angle and include this in least-squares fits (§ 5).

3.3. *Stokes Q and U*

A discussion similar to that of § 3.2 applies to Stokes Q and U, but it becomes more complicated because the measured values depend on parallactic angle PA, which changes with hour angle. That is, including the instrumental error terms we have

$$\begin{bmatrix} Q_{\mathrm{ant},n,j}(\nu) \\ U_{\mathrm{ant},n,j}(\nu) \end{bmatrix} = \boldsymbol{R}_n \cdot \begin{bmatrix} Q_{\mathrm{sky},n,j}(\nu) \\ U_{\mathrm{sky},n,j}(\nu) \end{bmatrix} + \begin{bmatrix} \Delta Q_{n,j}(\nu) \\ \Delta U_{n,j}(\nu) \end{bmatrix}, \tag{11a}$$

where

$$\boldsymbol{R}_n = \begin{bmatrix} \cos 2\mathrm{PA}_n & \sin 2\mathrm{PA}_n \\ -\sin 2\mathrm{PA}_n & \cos 2\mathrm{PA}_n \end{bmatrix}. \tag{11b}$$

Here we neglect the change in PA during a pattern, so the terms are subscripted only with n. As in the above discussion for V, for the purpose of the least-squares fit we must retain all of the unknowns, and none of the knowns, on the right-hand side of the equation. For the least-squares fit, the required equation is the analogy to equation (10d)

$$\begin{bmatrix} Q_{\mathrm{ant},n,j}(\nu) \\ U_{\mathrm{ant},n,j}(\nu) \end{bmatrix} - \boldsymbol{R}_n \cdot \begin{bmatrix} e^{-\tau_0(\nu)}Q_{\mathrm{sky},n,j} \\ e^{-\tau_0(\nu)}U_{\mathrm{sky},n,j} \end{bmatrix} = \boldsymbol{R}_n \cdot \left[\begin{bmatrix} Q'_{\mathrm{sky},n,j}(\nu) \\ U'_{\mathrm{sky},n,j}(\nu) \end{bmatrix}\right] + \begin{bmatrix} [\Delta Q_{n,j}(\nu)] \\ [\Delta U_{n,j}(\nu)] \end{bmatrix}. \tag{12}$$

We remind the reader that $Q_{\mathrm{sky},n,j}$ (no ν dependence) is the continuum value obtained from the off-line channels and is known quite accurately. The quantity $Q'_{\mathrm{sky}}(\nu)$, with the prime, is defined analogously to that for $V'_{\mathrm{sky}}(\nu)$ in equation (10c). As with V, the

quantities (not the matrices) in square brackets are solved by least squares. We either ignore the instrumental contributions and estimate their magnitudes, as discussed in § 8.2, or include their dependences on PA in the least-squares fit (§ 6.2).

For the continuum values of (Q, U), the major contributor to (ΔQ, ΔU) is zero offsets. We measure two polarized Stokes parameters, Stokes U and V, by cross-correlating the voltages of orthogonal polarizations and the third, Stokes Q, by differencing the powers of orthogonal polarizations (Heiles 2001). The last is particularly susceptible to instrumental problems, primarily a frequency-independent zero offset, both because the receiver temperatures differ and because the gains of the two polarizations are not perfectly calibrated. The shape of the spectrum can also be changed by the introduction of a weak replica of the Stokes I spectrum, but we ignore this because it is indeterminate. Even the cross-correlation spectra have small offsets because of instrumental coupling between the two channels, and these depend slightly on the Stokes I-value because of errors in the Müller matrix coefficients (see Heiles et al. 2001b).

These offset errors are frequency independent, so they affect only the continuum values. $\Delta U_{n,j}$, which is determined by cross-correlation, is smaller and more nearly constant than $\Delta Q_{n,j}$. In equations (10d) and (12), the quantities enclosed in square brackets are unknown and need to be determined by least-squares fitting. The number of unknowns is awkwardly large, as was the case for equation (9) in Paper I, and for the same reasons. We apply the same iterative technique here, namely neglecting the n-dependence of $Q_{\mathrm{sky},j}(\nu)$ and $U_{\mathrm{sky},j}(\nu)$ and first solving for the set of J-values for each spectral channel individually, and then solving for the NJ-values of $\Delta Q_{n,j}$ and $\Delta U_{n,j}$ using all channels and measurements simultaneously. Having done this, we correct the measured $Q_{\mathrm{ant},n,j}(\nu)$, $U_{\mathrm{ant},n,j}(\nu)$-values by subtracting the frequency-independent offsets $\Delta Q_{n,j}$ and $\Delta U_{n,j}$ and use those corrected values to proceed with the least-squares solution of equation (12), including frequency-dependent instrumental contributions as discussed in § 5.

4. INSTRUMENTAL PROBLEMS WITH POLARIZED STOKES PARAMETERS: GENERAL DISCUSSION

This section discusses the most important instrumental contributions to instrumental polarization. Polarized opacities are small, so we must consider systematic effects at very low levels. The most important contributors include the following:

1. There is instrumental coupling between the polarized Stokes parameters and Stokes I, which creates replicas of the Stokes I line in the polarized Stokes parameter spectra. These couplings are described by the Müller matrix (Heiles et al. 2001b) and are corrected for, but the corrections are imperfect.

Experience teaches us that this is usually the dominant instrumental contribution to the measured Stokes V spectra, typically amounting to a few tenths of a percent. Fortunately, in deriving Zeeman splitting its presence is unimportant: observers normally call this a "gain error" and use a least-squares technique to remove it.

2. The Müller matrix is derived from observations of small-diameter continuum sources, so it applies to beam center. However, it changes within the telescope beam. For Stokes V the primary effect is "beam squint," for which the V beam has positive and negative lobes on opposite side of beam center. This arises from the two polarizations pointing in slightly different directions. Beam squint interacts with the first spatial derivative of the Stokes I profile to produce a false contribution. We assume that the beam squint is fixed with respect to the feed, so its false contribution varies periodically with the parallactic angle PA.

Beam squint is theoretically predicted to occur for Stokes V but not for Q and U. However, Arecibo has significant beam squint in Q and U as measured by the response to the first spatial derivative in Stokes I; it is probably produced by the significant aperture blockage. Figures 12, 13, and 14 of Heiles et al. (2001a) show that the effective beam squint for both Q and U is about 10 times that for V.

Beam squint correlates with the angular structure in the *emission* line to produce unreal features in the *polarized* Stokes emission and absorption spectra. Experience shows that for Stokes V, beam squint interacting with the first derivative of H I intensity is the most serious instrumental problem (Heiles 1996). For conventional telescopes this contribution can be measured and removed rather accurately. For the Arecibo telescope, however, the polarized beam pattern changes partly systematically, partly erratically with hour angle, making the correction impractical.

We can estimate the magnitude of this contribution from the measured angular derivatives of the Stokes I expected profile and the approximately known magnitude of the beam squint (§ 8.2). Also, we can determine the approximate contribution by fitting for the change in the apparent polarized opacity spectrum as the polarized beam rotates with respect to the sky with hour angle (§ 5). However, because Arecibo's beam characteristics, including squint, change while tracking, the squint contribution varies not only with PA but also has a semirandom component. We least-squares fit equations (13a)–(13b) for the systematic squint component, as discussed below, but the semirandom component remains.

3. For Stokes Q and U, the primary effect for the polarized beam is "beam squash," for which the polarized beams have a four-lobed cloverleaf pattern, with two positive lobes on opposite side of beam center and two negative ones rotated 90°. This arises from the two polarizations having slightly different beam widths. Beam squash interacts with the second spatial derivative of the Stokes I emission profile to produce a false contribution that varies periodically with twice the parallactic angle 2PA.

Beam squash is theoretically predicted to occur for Stokes Q and U, but not for V. However, Arecibo, with its significantly blocked aperture, violates this rule. As with beam squint, Figures 12, 13, and 14 of Heiles et al. (2001a) show that Arecibo's effective beam squash for both Q and U is about 10 times that for V.

For Stokes V, most telescopes have negligible beam squash, so our experience with them does not apply to Arecibo. We can estimate the magnitude of the squash contribution from the measured angular derivatives of the Stokes I expected profile and the approximately known magnitude of the beam squash (§ 8.2). Also, we can approximately determine the contribution by fitting for the change in the apparent polarized spectrum as the polarized beam rotates with respect to the sky with hour angle (§ 5); this works well for the opacity spectrum. However, it does not work well for the expected emission spectrum because of the incomplete PA coverage (§ 8).

For Stokes Q and U we can estimate the squash contribution from the measured spatial derivatives and the known beam squash. However, we cannot determine it by fitting for the change with 2PA because real linear polarization also varies with 2PA.

4. All four Stokes parameters are affected by "far-out sidelobes," i.e., sidelobes outside the first sidelobe. These arise primarily from ordinary diffraction and, secondarily, from surface inaccuracies. Far-out sidelobes for Arecibo are particularly strong because of the severe aperture blockage; and they contribute disproportionately to the squint and squash response. They are likely to be polarized comparably to the first sidelobe, and the H I spatial structure within them changes more because the angular differences are larger; this magnifies their importance. The first sidelobe itself serves as an illustration: for a uniform extended source in Stokes I, it contributed 0.34 as much as the primary beam in 2000[3]); yet in Stokes V it contributed almost *twice* as much to the observed squint response as does the primary beam! (see Table 1 and Figure 14 of Heiles et al. 2001a).

Far-out sidelobes can, like squint and squash, be expressed as a Fourier series in PA. The first term is squintlike, and the second is squashlike. Below, we use the terms "squintlike" and "squashlike" to denote the contribution from the telescope, i.e., from the primary beam and all sidelobes, and unless the context dictates otherwise we use the terms "squint" and "squash" to denote the contributions from the primary beam and first sidelobe.[4]

Contribution (1) produces only a replica of the Stokes I opacity profile; in Zeeman splitting this is routinely removed by least-squares fitting and has no damaging effect. Accordingly, we do not consider it further.

The contributions (2), (3), and (4) exhibit sinusoidal dependences on either PA (squintlike) or 2PA (squashlike). There are two independent ways to evaluate these contributions, each with its own problem. The *empirical* way (§ 5) is observing a range of PA and performing a least-squares fit on the results to directly evaluate (and remove) the sinusoidal dependences; the problem, especially for the emission profile, is the incomplete PA coverage. The other way (§ 8.2) *predicts* the instrumental effects using the angular derivatives of the H I structure in the sky, together with the already known polarization structures of the Arecibo beam; the problem is the neglect of the far-out sidelobe contribution. We turn to a detailed discussion of these issues in the next few sections.

5. EMPIRICAL EVALUATION OF SQUINTLIKE AND SQUASHLIKE CONTRIBUTIONS TO STOKES V OPACITY SPECTRA

Squintlike structure in the Stokes V polarized beam interacts with the first spatial derivative of the Stokes I profile to produce a false contribution to V that varies periodically with the parallactic angle PA, and squashlike structure interacts with the second spatial derivative to produce a contribution that varies periodically with 2 PA. Here we follow Heiles (1996) in using least-squares fitting to empirically evaluate both contributions. If we had complete and uniform PA coverage these fits would be straightforward, but this is not the case.

Beam squintlike and squashlike structure produce instrumental contributions $\Delta V_{n,j}(\nu) = V_{\mathrm{sqnt},n,j}(\nu)$ and $V_{\mathrm{sqsh},n,j}(\nu)$, respectively, where $\Delta V_{n,j}(\nu)$ is the instrumental contribution in equation (10d). We parameterize these as follows:

$$V_{\mathrm{sqnt},n}(\nu) = [V_{\mathrm{sqnt,cos}}(\nu)]\cos(\mathrm{PA}_n) + [V_{\mathrm{sqnt,sin}}(\nu)]\sin(\mathrm{PA}_n), \tag{13a}$$

$$V_{\mathrm{sqsh},n}(\nu) = [V_{\mathrm{sqsh,cos}}(\nu)]\cos(2\mathrm{PA}_n) + [V_{\mathrm{sqsh,sin}}(\nu)]\sin(2\mathrm{PA}_n). \tag{13b}$$

Again, the square brackets indicate the unknown quantities to be determined by least squares. Note that the continuum quantities do not appear in this equation; this is because the squint and squash contributions arise only from the H I *emission* in the vicinity of the source (as long as the continuum source is small compared to the beam), so the source intensity is irrelevant. Moreover, we are assuming no spatial gradients in $V_{\mathrm{sqnt,\,cos}}$ and $V_{\mathrm{sqnt,\,sin}}$, so have dropped the subscript j.

Least-squares fitting equations (10a)–(10d) allows us to solve for six unknowns, i.e., the two contained in $V'_{\mathrm{sky}}(\nu)$ in equation (10c) together with the four instrumental ones in equations (13a)–(13b), as long as we cover a sufficiently large range in PA. At Arecibo, the maximum PA range is $\sim 180^\circ$; for other alt-az telescopes, a significantly larger range is available only for sources that are nearly circumpolar.

Figure 1 shows the PA coverage for our example of 3C 138, which is unusual in having rather sparse PA coverage. This sparse coverage occurs for two reasons: first, the declination of 3C 138 differs from Arecibo's latitude by only $\sim 2^\circ$, which means that the PA changes rapidly near transit. Thus, as the source is observed and the PA increases from $\sim 90^\circ$ to $\sim 270^\circ$ (same as -90°), a broad band of PA centered near 180° is not sampled. Second, the exigencies of scheduling meant that it received little time at negative hour angles. Most sources have more complete coverage. We choose 3C 138 as the example because its incomplete PA coverage highlights the associated difficulties and because the angular derivatives of brightness temperature are unusually high, which exacerbates instrumental effects.

The incomplete PA coverage has different ramifications for the derived expected and opacity profiles:

1. For the expected emission spectrum $V_{\mathrm{exp}}(\nu)$ the effects of incomplete PA coverage are serious. Five terms in equation (10a) are independent of being on- or off-source. These are the five emission-profile terms, namely, $V_{\mathrm{exp}}(\nu)$ in equations (10a)–(10d) and the four terms in equations (13a)–(13b). These five terms constitute the first three frequency components of a sin/cosine Fourier series with real coefficients. If the PA coverage were complete and uniform, covering the *full* range of 360° with uniform sampling, then the least-squares solution of equation (10a) would be identical to a regularly sampled Fourier transform in which the five terms are orthogonal and therefore independent. The incomplete coverage of $\lesssim 180^\circ$ is a problem because it removes this orthogonality. The nonorthogonality produces coupling between all five terms and, also, extra noise. We will refer to this problem in the ensuing discussion under the rubric "covariance."

2. For the opacity spectrum $\tau'_V(\nu)$ the effects of incomplete PA coverage are much less serious. The reason is simply that $\tau'_V(\nu)$ is, fundamentally, the ON-OFF spectrum and the continuum source is strong: the PA coverage enters only peripherally. There is little covariance between $\tau'_V(\nu)$ and the other five terms discussed above.

[3] Arecibo's surface was readjusted and the focus point changed in 2002. The current fraction is much lower, $\lesssim 0.10$.

[4] To be precise, true squint and squash refer only to the main beam without the first sidelobe. But Heiles et al. (2001a) measured the influence of both—for Arecibo, the first sidelobe is large because of the large aperture blockage. For this reason, in this paper we stretch the definition of "true."

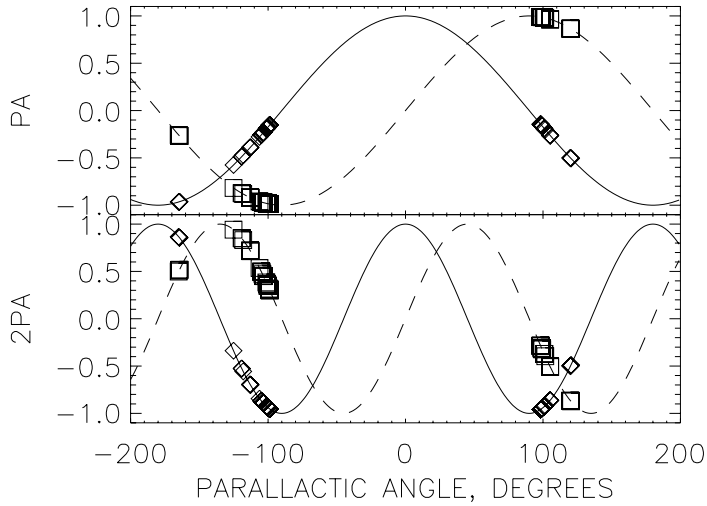

FIG. 1.—Trigonometric functions (*solid line*, cosine; *dashed line*, sine) of PA and 2 PA vs. PA. The squares and diamonds depict the actual observed PA-values for 3C 138 and illustrate the absence of complete coverage.

5.1. *Stokes V: General Discussion*

We have our choice in what to include for $\Delta V_{n,j}(\nu)$ in the least-squares fits to equations (10a)–(10d). We could fit by ignoring both the squintlike and squashlike contributions, i.e., setting $\Delta V_{n,j}(\nu) = 0$; we denote these solutions for the two unknowns $V_{\rm exp}(\nu)$ and $\tau'_V(\nu)$ in equation (10d) with the additional subscript 0. We could include only the squintlike terms in $V_{\rm sqnt}(\nu)$, for which we have four unknowns (the original two plus $[V_{\rm sqnt,cos}(\nu)]$ and $[V_{\rm sqnt,sin}(\nu)]$), for which the additional subscript is 1; or we could include both squintlike and squashlike terms, for which we have six unknowns and the additional subscript is 2.

The instrumental contributions in these three cases are most concisely expressed by matrix equations that give the contribution to the two derived quantities $[V_{\rm exp}(\nu)$ and $\tau'_V(\nu)]$ in equations (10a)–(10d) in terms of the two true ones and, in addition, the four true squint and squash ones in equations (13a)–(13b). Here, by "true" we mean the values that actually occur, which are not equal to the ones derived by the least-squares fit because of the covariance caused by incomplete PA coverage. We calculate these matrix elements by inserting known artificial signals into the data and calculating the resulting contributions. For example, to evaluate the effect of $V_{\rm sqsh,cos,true}$, we insert the artificial signal $\cos(2{\rm PA}_{n,j})$ into spectral channel number 2 (which contains no useful astronomical information) and process it identically to the other spectral channels; the resulting values of τ'_V, $V_{\rm exp}$, etc., provide the corresponding matrix elements. The matrix elements are the approximate coupling coefficients between a given derived quantity, such as τ'_V, and the squintlike and squashlike instrumental effects as embodied in, for example, $V_{\rm sqsh,cos,true}$. These coefficients differ for each source because of the differing PA coverage. In these fits, we assume $\tau_0(\nu) = 0$; the matrix elements depend somewhat on $\tau_0(\nu)$, so the particular values shown below are only representative.

We outline the three cases in the following subsections.

5.1.1. *Least-Squares Fitting Including neither Squint nor Squash*

First, we derive $\tau'_{V,0}(\nu)$ and $V_{\rm exp,0}(\nu)$ by not fitting for squint and squash, i.e., by least-squares fitting equation (10d) setting the instrumental $\Delta V_{n,j}(\nu) = 0$. For 3C 138, this gives

$$\begin{bmatrix} \tau'_{V,0} \\ V_{\rm exp,0} \end{bmatrix} = \begin{bmatrix} 1.01 & 6.8{\rm E}-5\ {\rm K}^{-1} & -6.7{\rm E}-5\ {\rm K}^{-1} & -1.1{\rm E}-5\ {\rm K}^{-1} & -2.1{\rm E}-5\ {\rm K}^{-1} & -3.3{\rm E}-5\ {\rm K}^{-1} \\ +3.8\ {\rm K} & 0.98 & -0.29 & -0.21 & -0.74 & +0.12 \end{bmatrix} \times \begin{bmatrix} \tau'_{V,\rm true} \\ V_{\rm exp,true} \\ V_{\rm sqnt,cos,true} \\ V_{\rm sqnt,sin,true} \\ V_{\rm sqsh,cos,true} \\ V_{\rm sqsh,sin,true} \end{bmatrix}. \tag{14}$$

First we discuss $\tau'_{V,0}$, whose matrix elements are in the first row. The first matrix element, 1.01, reflects the fact that our least-squares solution for $\tau'_{V,0}$ actually works and returns the correct value. The second expresses the contribution of real Zeeman splitting in the expected emission profile $[V_{\rm exp}(\nu)]$ to the derived $\tau'_{V,0}$, and the remaining ones express the instrumental (fake) contributions arising from the polarized beam interacting with spatial derivatives in $[I(\nu)]$. The numerical values for these last five matrix elements have upper limits, which we obtain as follows. From equations (7b) and (10b), we find that the opacity $\tau'_V(\nu) = V(\nu)/I_{\rm src}$. For 3C 138, $I_{\rm src} \approx 116$ K, so in calculating $\tau'_{V,0}(\nu)$ the instrumental contribution $V(\nu)$ gets multiplied by $\sim 1/116 = 8.5 \times 10^{-3}$ K^{-1}. This is the upper limit for the last five matrix elements, and it is well above the actual values.

In particular, all of the matrix elements on the first row (except the first) are inversely proportional to the continuum source intensity: the stronger the source, the weaker the instrumental contribution to τ'_V. This large reduction in instrumental effects is one reason why Arecibo, with its huge collecting area, is the instrument of choice for these single-dish absorption studies.

Now we discuss $V_{\mathrm{exp},0}$, whose matrix elements are in the second row. Again, the second matrix element, 0.98, reflects the fact that our least-squares solution for $V_{\mathrm{exp}}(\nu)$ returns the correct value. Regarding the squint and squash terms, this least-squares calculation of $V_{\mathrm{exp},0}$ ignores all PA variation and is therefore equivalent to an average of all the measured values. The third matrix element (which multiplies $V_{\mathrm{sqnt,cos,true}}$) equals -0.29. This must equal the average value of $\cos(\mathrm{PA})$ because any nonzero value of $V_{\mathrm{sqnt,cos,true}}$ contributes this fractional amount in a straight average. Visual inspection of Figure 1 confirms this expectation. Similarly, the sine component $V_{\mathrm{sqnt,cos,true}}$ equals -0.21. This component has the possibility of being nearly zero if the source has symmetric hourangle coverage, because $\sin(\mathrm{PA})$ is antisymmetric; indeed, this is the case for many of our sources—but not for 3C 138 because of the exigencies of scheduling.

5.1.2. *Least-Squares Fitting Including Squint but not Squash*

Next, we least-squares fit equation (10d) including only the two squintlike terms in equations (13a)–(13b) and ignoring squash. The matrix becomes

$$\begin{bmatrix} \tau'_{V,1} \\ V_{\mathrm{exp},1} \\ V_{\mathrm{sqnt,cos},1} \\ V_{\mathrm{sqnt,sin},1} \end{bmatrix} = \begin{bmatrix} 1.01 & +6.8\mathrm{E}-5\ \mathrm{K}^{-1} & -5.4\mathrm{E}-5\ \mathrm{K}^{-1} & -7.2\mathrm{E}-5\ \mathrm{K}^{-1} & -4.8\mathrm{E}-5\ \mathrm{K}^{-1} & -9.1\mathrm{E}-6\ \mathrm{K}^{-1} \\ +4.7\ \mathrm{K} & 0.99 & 0 & 0 & -1.33 & -0.10 \\ +3.1\ \mathrm{K} & 0.02 & 0.98 & 0 & -2.02 & -0.40 \\ -0.2\ \mathrm{K} & 0 & 0 & 0.99 & 0 & -0.48 \end{bmatrix} \times \begin{bmatrix} \tau'_{V,\mathrm{true}} \\ V_{\mathrm{exp,true}} \\ V_{\mathrm{sqnt,cos,true}} \\ V_{\mathrm{sqnt,sin,true}} \\ V_{\mathrm{sqsh,cos,true}} \\ V_{\mathrm{sqsh,sin,true}} \end{bmatrix}. \tag{15}$$

First we discuss $\tau'_{V,1}$. Comparison of the third and fourth elements in the top rows of equations (14) and (15) shows that including the squint changes the contributions to $\tau'_{V,1}$ by factors of 0.8 and 6.5 for the cosine and sine components, respectively. The sine component contributes more to $\tau'_{V,1}$ than to $\tau'_{V,0}$, which is surprising. As we noted above, 3C 138 has asymmetric PA coverage; sources having more nearly symmetric PA coverage exhibit large reductions in the squint contribution to $\tau'_{V,1}$. For example, 3C 207 has nearly symmetric coverage and the factors above are much smaller—0.3 and 0.02, respectively.

Now we discuss $V_{\mathrm{exp},1}$. Because we explicitly fit for them here, the $V_{\mathrm{exp},1}(\nu)$ (second row) matrix elements of both components of $V_{\mathrm{sqnt,true}}$ (i.e., the third and fourth elements) are essentially zero. However, there is a large covariance between $\cos(\mathrm{PA})$ and $\cos(2\mathrm{PA})$ for the incompletely sampled PA range, which leads to the large value of -1.33 for the matrix element for $V_{\mathrm{sqsh,cos,true}}$. It is surprising that this element exceeds unity. Similarly, the last two matrix elements for $V_{\mathrm{sqnt,\ cos\ ,1}}$ also exceed unity. Such surprises can occur when fitting nonorthogonal functions with high covariance (these functions being the incompletely sampled trigonometric functions of PA and 2PA).

5.1.3. *Least-Squares Fitting Including both Squint and Squash*

Finally, we least-squares fit equation (10d) including both the two squintlike and squashlike terms in equations (13a)–(13b). Then we get

$$\begin{bmatrix} \tau'_{V,2} \\ V_{\mathrm{exp},2} \\ V_{\mathrm{sqnt,cos},2} \\ V_{\mathrm{sqnt,sin},2} \\ V_{\mathrm{sqsh,cos},2} \\ V_{\mathrm{sqsh,sin},2} \end{bmatrix} = \begin{bmatrix} 1.01 & +6.8\mathrm{E}-5\ \mathrm{K}^{-1} & -5.4\mathrm{E}-5\ \mathrm{K}^{-1} & -7.2\mathrm{E}-5\ \mathrm{K}^{-1} & -6.3\mathrm{E}-5\ \mathrm{K}^{-1} & +1.1\mathrm{E}-5\ \mathrm{K}^{-1} \\ +4.4\ \mathrm{K} & 1.02 & 0 & +0.01 & -0.05 & -0.01 \\ +2.7\ \mathrm{K} & +0.06 & 0.98 & +0.01 & -0.08 & -0.01 \\ 0\ \mathrm{K} & +0.01 & 0 & 1.00 & -0.01 & -0.01 \\ -0.3\ \mathrm{K} & +0.02 & 0 & 0 & 0.96 & 0 \\ +0.3\ \mathrm{K} & 0 & 0 & +0.02 & -0.01 & 0.98 \end{bmatrix} \times \begin{bmatrix} \tau'_{V,\mathrm{true}} \\ V_{\mathrm{exp,true}} \\ V_{\mathrm{sqnt,cos,true}} \\ V_{\mathrm{sqnt,sin,true}} \\ V_{\mathrm{sqsh,cos,true}} \\ V_{\mathrm{sqsh,sin,true}} \end{bmatrix}. \tag{16}$$

For $\tau'_{V,2}$, including squash gives a modest degradation for the two squash terms (the last two matrix elements in the top row). More impressively, for $V_{\mathrm{exp},2}$ the large squash contributions to $V_{\mathrm{exp},1}$ in equation (15) (the last two matrix elements in the second row) are changed by factors of $\sim$0.04 and 0.1. This desired elimination of the squint and squash contributions to $V_{\mathrm{exp},2}$ comes at a heavy price. As we shall see in § 8 and Figure 5, the spectrum $V_{\mathrm{exp},2}$ is much noisier than for $V_{\mathrm{exp},0}$ and $V_{\mathrm{exp},1}$; unfortunately, this means that we cannot provide reliable Stokes V spectra for the emission spectra. The excess noise is again the covariance caused by the incomplete PA coverage. As is true with any least-squares fit, coefficients having high covariance are determined with large errors.

Comparison of the above matrices shows that we can significantly improve our resistance to instrumental effects by observing as full and complete PA range as possible. Because most sources have better complete PA coverage than 3C 138, their opacity profiles $\tau'_{V,2}$ have smaller instrumental contributions than either $\tau'_{V,0}$ or $\tau'_{V,1}$. Accordingly, we shall include both squintlike and squashlike terms in the fit to equation (10d) and always present $\tau'_{V,2}$. The derived quantity $\tau'_{V,2}$ automatically has the squintlike and squashlike contributions removed.

5.2. *Instrumental Contributions to $\tau'_V(\nu)$ for the Example of 3C 138*

5.2.1. *Stokes V: the Data*

We illustrate these concepts by showing and discussing the instrumental contributions to the $\tau'_V(\nu)$ spectra for 3C 138. We choose 3C 138 because it is one of the few sources to exhibit a clearly detectable signal in $\tau'_V(\nu)$ and because its PA coverage is not very good, so it should represent a less-than-optimum case.

Figure 2 illustrates three derived spectra for $\tau'_V(\nu)$. The first (*top*) panel is the classical opacity spectrum $e^{-\tau_0(\nu)}$. The second panel is $\tau'_{V,0}(\nu)$, which is derived not fitting for squint and squash, i.e., least-squares fitting equation (10d) with $\Delta V_{n,j} = 0$; this is equivalent to the standard ON-OFF spectrum. The third panel is $\tau'_{V,2}(\nu)$, which is derived including both squintlike and squashlike terms in equations (13a)–(13b). We do not show $\tau'_{V,1}(\nu)$ because it is indiscernibly different from $\tau'_{V,2}(\nu)$. Even $\tau'_{V,0}(\nu)$ and $\tau'_{V,2}(\nu)$ in the second and third panels are almost identical; the fourth panel shows the difference on a 10 times expanded scale. The similarity of $\tau'_{V,0}(\nu)$ and $\tau'_{V,2}(\nu)$ is a clear indication that neither squintlike nor squashlike effects contribute significantly to the Stokes V opacity profile for 3C 138.

5.2.2. *Stokes V: Evaluation of Matrix Products for the Example of 3C 138*

We can evaluate the approximate instrumental contribution of the $V(\nu)$ emission terms to $\tau'_{V,2}(\nu)$. These instrumental contributions $\delta\tau'_V(\nu, 2)$ are given by equation (16), viz.,

$$\left[\delta\tau'_{V,2}\right] = \left[\begin{array}{cccccc} 0 & +6.8\mathrm{E}-5\ \mathrm{K}^{-1} & -5.4\mathrm{E}-5\ \mathrm{K}^{-1} & -7.2\mathrm{E}-5\ \mathrm{K}^{-1} & -6.3\mathrm{E}-5\ \mathrm{K}^{-1} & +1.1\mathrm{E}-5\ \mathrm{K}^{-1} \end{array}\right] \times \begin{bmatrix} \tau'_{V,\mathrm{true}} \\ V_{\mathrm{exp,true}} \\ V_{\mathrm{sqnt,cos,true}} \\ V_{\mathrm{sqnt,sin,true}} \\ V_{\mathrm{sqsh,cos,true}} \\ V_{\mathrm{sqsh,sin,true}} \end{bmatrix}. \tag{17}$$

From the lower two panels of Figures 6 and 7, we crudely estimate

$$\begin{bmatrix} \tau'_{V,\mathrm{true}} \\ V_{\mathrm{exp,true}} \\ V_{\mathrm{sqnt,cos,true}} \\ V_{\mathrm{sqnt,sin,true}} \\ V_{\mathrm{sqsh,cos,true}} \\ V_{\mathrm{sqsh,sin,true}} \end{bmatrix} \sim \begin{bmatrix} \cdots \\ \cdots \\ 0.7\ \mathrm{K} \\ 0.1\ \mathrm{K} \\ 0.2\ \mathrm{K} \\ 0.2\ \mathrm{K} \end{bmatrix}. \tag{18}$$

These numerical estimates are zero-to-peak, not peak-to-peak.

We have not specified the contribution from $V_{\mathrm{exp,true}}$ because we cannot measure it accurately (see § 8). However, we can estimate it. The Zeeman splitting in the emission line is likely to be comparable to that in the absorption line. That is, loosely speaking we expect $V_{\mathrm{exp}}(\nu)/T_{\mathrm{exp}}(\nu) \sim \tau'_{V,2}(\nu)/\tau_0(\nu)$. Roughly, if $\tau_0(\nu) \lesssim 1$, then $T_{\mathrm{exp}}(\nu) \approx T_s\tau_0(\nu)$, where T_s is the spin temperature. This gives

$$V_{\mathrm{exp}}(\nu) \sim T_s\tau'_{V,2}(\nu). \tag{19}$$

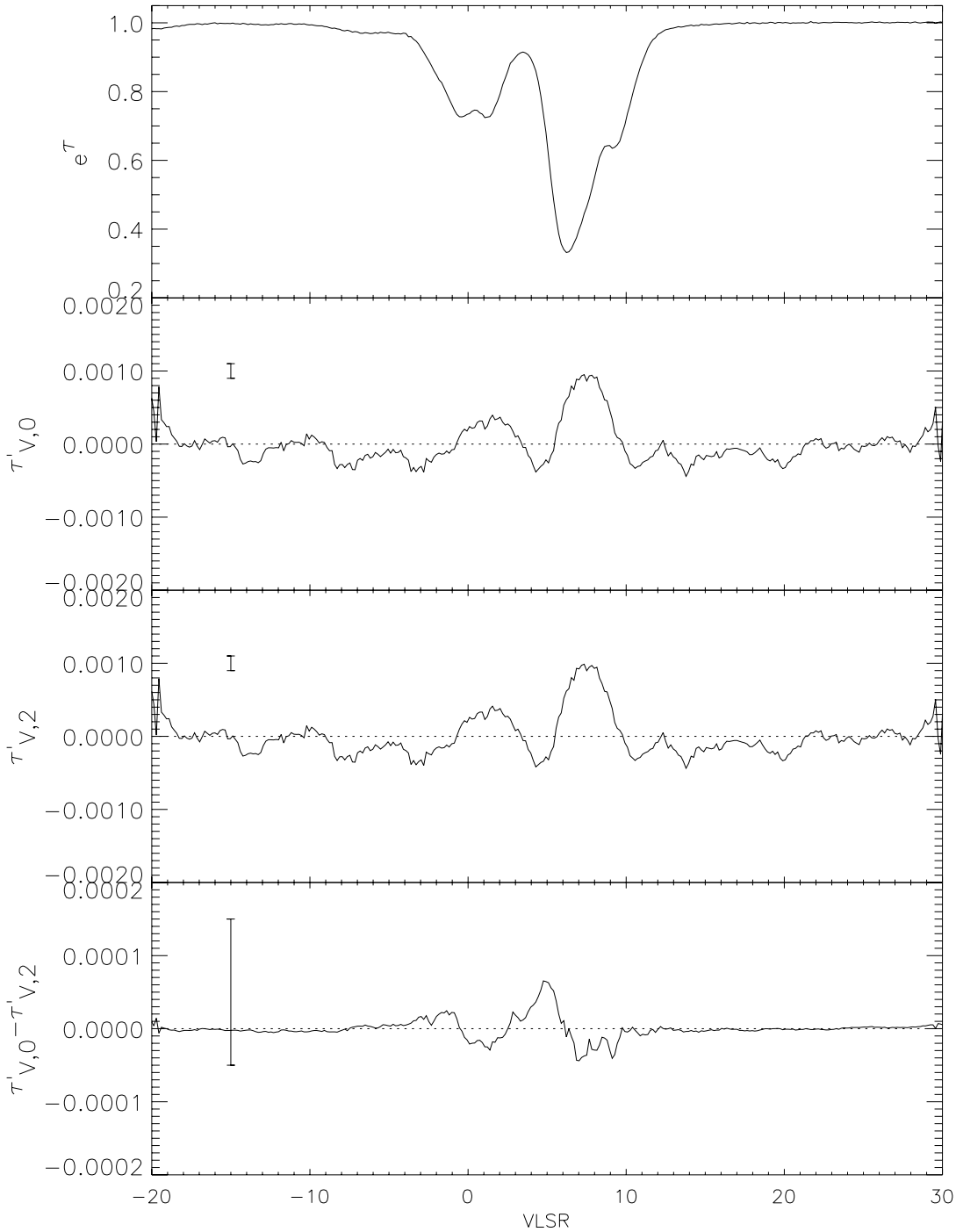

FIG. 2.—*I* and *V* opacity spectra for 3C 138. The first (*top*) panel is $e^{-\tau_0(\nu)}$. The second panel is $\tau'_{V,0}(\nu)$, derived by ignoring squint and squash; the third is $\tau'_{V,2}(\nu)$, derived including both squint and squash; and the fourth is the difference $\tau'_{V,0}(\nu) - \tau'_{V,2}(\nu)$. The spectra in the bottom three panels are boxcar smoothed by nine channels to reduce the noise. As shown by the sample error bar, the scale on the bottom panel is expanded by a factor of 10.

We obtain the contribution of $V_{\rm exp}(\nu)$ to $\delta\tau'_{V,2}(\nu)$ by multiplying the above equation (19) by the corresponding matrix element (the second element in eq. [17]). This yields a contribution

$$\frac{\delta\tau'_{V,2}(\nu)}{\tau'_{V,2}(\nu)} \sim 6.8 \times 10^{-5} T_s \lesssim 6.8 \times 10^{-3}, \tag{20}$$

where we have assumed $T_s = 100$ K for this estimate, which is generously high given the results of Paper II. Therefore, the fractional contribution $\delta\tau'_{V,2}(\nu)/\tau'_{V,2}(\nu)$ is negligible for any source flux and we can neglect the contribution of $V_{\rm exp}(\nu)$.

To get a rough estimate of the maximum total instrumental contribution from squintlike and squashlike effects, we add the absolute values of the four individual contributions in equation (18). We obtain $\delta\tau'_{V,2} \lesssim 6 \times 10^{-5}$. This is comparable to the last panel in Figure 2; both are about 20 times smaller than the detected Zeeman splitting in 3C 138. This is comfortably small. These instrumental contributions scale inversely with source flux density S. For all sources our plots (e.g., Fig. 9) exhibit equation (16)'s matrix product for $\delta\tau'_{V,2}(\nu)$. The profile $\delta\tau'_{V,2}(\nu)$ represents the approximate channel-by-channel instrumental contribution to the Stokes V opacity profile resulting from all squintlike and squashlike contributions. In no case is this contribution significant compared to $\tau'_{V,2}(\nu)$. This is fortunate, because it means that even if $\delta\tau'_{V,2}(\nu)$ is not well determined, subtracting its contribution incurs little loss of accuracy in the final result $\tau'_{V,2}(\nu)$.

6. EMPIRICAL EVALUATION OF SQUINTLIKE AND SQUASHLIKE CONTRIBUTIONS TO STOKES (Q, U) OPACITY SPECTRA

In their discussion of polarized sidelobes, Heiles et al. (2001a) provide numerical coefficients for true squint and squash of Stokes (Q, U). These coefficients are about 10 times larger than for Stokes V. We believe that squint and squash are representative samples of all polarized beam effects, so that this indicates that all sidelobes are more serious in linear than circular polarization. Specifically, we assume that this factor of 10 applies not just to true squint and squash, but also to squintlike, squashlike, and all other types of sidelobe contribution.

The polarized spectra $\tau'_{Q,1}(\nu)$ and $\tau'_{U,1}(\nu)$ should be zero unless there is opacity structure in the H I that varies across the source together with continuum polarization that also varies across the source. If we assume that there is no such structure, then any nonzero behavior in $\tau'_{Q,1}(\nu)$ and $\tau'_{U,1}(\nu)$ must result from the instrumental contribution of polarized sidelobes. Dividing these by 10 provides an estimate of the instrumental contribution to Stokes $\tau'_{V,2}(\nu)$.

6.1. *Stokes (Q, U): General Discussion*

Stokes Q and U are more complicated to treat than V because the sky values are rotated as in equation (11a). Moreover, we cannot fit for squashlike behavior because its PA-dependence is identical to that of real linear polarization. After performing the correction for the continuum offsets described in § 3.3, we are left with

$$\begin{bmatrix} [\Delta Q_n(\nu)] \\ \Delta U_n(\nu) \end{bmatrix} = \begin{bmatrix} [Q_{\mathrm{sqnt,cos}}(\nu)] \cos \mathrm{PA}_n + [Q_{\mathrm{sqnt,sin}}(\nu)] \sin \mathrm{PA}_n \\ [U_{\mathrm{sqnt,cos}}(\nu)] \cos \mathrm{PA}_n + [U_{\mathrm{sqnt,sin}}(\nu)] \sin \mathrm{PA}_n \end{bmatrix}, \tag{21}$$

where, as with V in equations (13a)–(13b), we have dropped the j subscript because we assume spatial derivatives are zero.

We could derive matrix elements for Stokes (Q, U) as we did for V in equations (14) and (15) (we cannot derive those for squashlike behavior). However, we will not do this. The matrix elements depend on the PA coverage and Stokes I; the only difference between linear and circular polarization is the necessity to include the additional PA dependencies in equations (11a) and (21), and the matrix elements for (Q, U) would be comparable in magnitude to those for V but different in detail. Owing to the illustrative nature of our discussion, it is not worth taking up this space.

6.2. *Examples of Observed Linear Polarization* $[\tau'_Q(\nu), \tau'_U(\nu)]$

6.2.1. *The Example of 3C 138*

Figure 3 illustrates the derived spectra for $\tau'_Q(\nu)$ and $\tau'_U(\nu)$. The first (*top*) panel shows the classical opacity spectrum $e^{-\tau_0(\nu)}$. The second (*middle*) panel shows $\tau'_{Q,1}(\nu)$ and $\tau'_{U,1}(\nu)$, which are derived including the squint, i.e., least-squares fitting equation (12) with ($\Delta Q_{n,j}$, $\Delta U_{n,j}$) given by equation (21).

The two spectra in the middle panel show features with peak excursion $\sim$0.015. However, their shapes mimic to some degree the shape of the Stokes I opacity profile $\tau_0(\nu)$ in the top panel. This similarity in shape is probably the result of a small error in the Müller matrix coefficients, causing Stokes I to leak into Q and U at the level of a few tenths of a percent. This is the gain error discussed in item 1 of § 4.

The bottom panel of Figure 3 shows gain-corrected spectra of $\tau'_Q(\nu)$ and $\tau'_U(\nu)$. We fitted the two middle-panel spectra to $\tau_0(\nu)$ on a channel-by-channel basis; the dashed lines in the middle panel are the fits. The bottom panel shows the residuals [$\Delta\tau'_{Q,1}(\nu)$, $\Delta\tau'_{U,1}(\nu)$], i.e., the data minus the fitted points. These residual profiles are the results with the gain error removed, and should be zero. They are, in fact, zero except for bumps at the $\sim$0.003 level.

Under our assumption of zero true polarization, these $\sim$0.003 bumps must be the instrumental contribution from polarized sidelobes. Moreover, this instrumental contribution must arise from non-squintlike contributions because squintlike behavior has been removed from $\tau'_{Q,1}(\nu)$ and $\Delta\tau'_{U,1}(\nu)$. There are four possible production mechanisms for these bumps. The first is that there really is true linear polarization, i.e., that the true values of $\tau'_{Q,\mathrm{true}}(\nu)$ and/or $\tau'_{U,\mathrm{true}}(\nu)$ are not equal to zero. We will first dispose of this possibility by considering a different source, 3C 454.3.

6.2.2. *The Example of 3C 454.3*

3C 454.3 is a particularly useful source for understanding linearly polarized sidelobes because it is a VLBI calibrator and has a very small angular size ($\sim$14 milliarcsec; Fomalont et al. 2000; this is about 1000 times smaller than 3C 138). Despite the existence of tiny scale atomic structure (reviewed by Heiles 1997), we expect $\tau'_Q(\nu)$ and $\tau'_U(\nu)$ to be very small. We assume that any departure from zero is an instrumental contribution from polarized sidelobes.

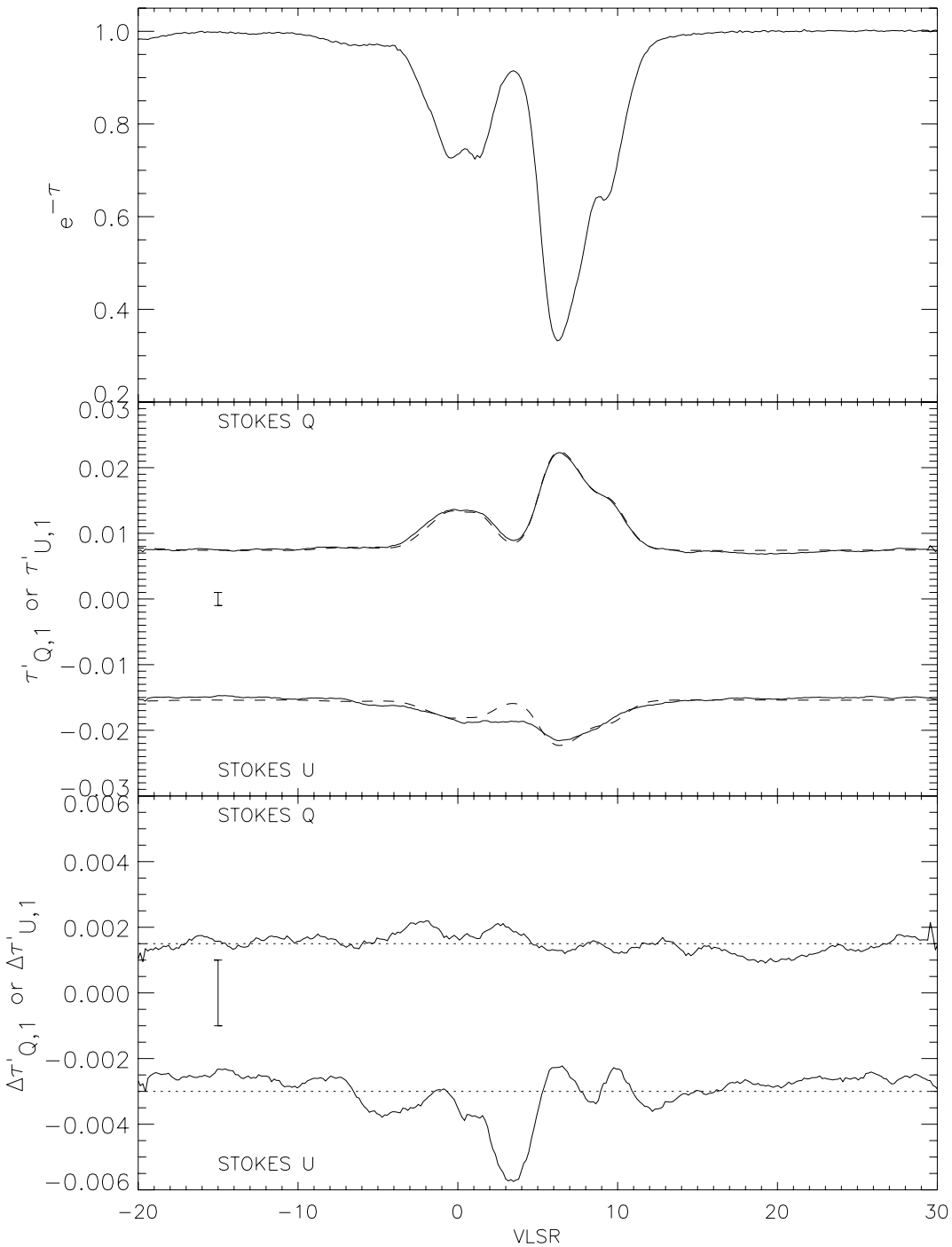

FIG. 3.—I and (Q, U) spectra for 3C 138. The first (*top*) panel is $e^{-\tau_0(\nu)}$. The second panel shows $\tau'_{Q,1}(\nu)$ and $\tau'_{U,1}(\nu)$, derived including squint and ignoring squash. The dashed lines are the fits of the $e^{-\tau_0(\nu)}$ spectra to the $\tau'(\nu)$ spectra. The bottom panel shows the "gain-corrected" versions of $\tau'_{Q,1}(\nu)$ and $\tau'_{U,1}(\nu)$, equal to the difference between the solid and dashed lines in the second panel. Spectra in the bottom two panels have displaced zeros and are boxcar smoothed by nine channels for clarity.

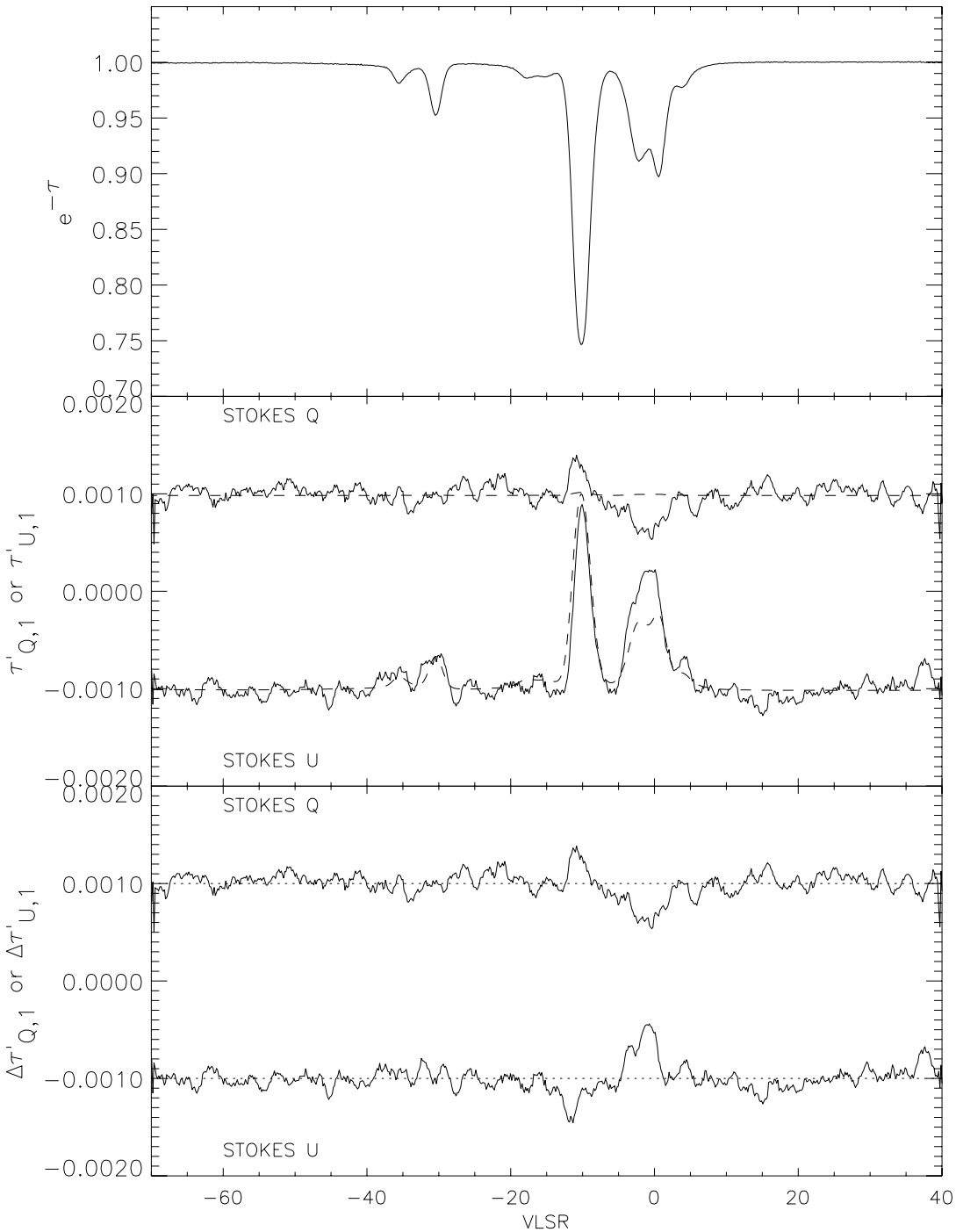

FIG. 4.—3C 454.3 analog of Fig. 3. The first (*top*) panel is $e^{-\tau_0(\nu)}$. The second panel shows $\tau'_{Q,1}(\nu)$ and $\tau'_{U,1}(\nu)$, derived including squint and ignoring squash. The dashed lines are the fits of the $e^{-\tau_0(\nu)}$ spectra to the $\tau'(\nu)$ spectra. The bottom panel shows the "gain-corrected" versions of $\tau'_{Q,1}(\nu)$ and $\tau'_{U,1}(\nu)$, equal to the difference between the solid and dashed lines in the second panel. Spectra in the bottom two panels have displaced zeros and are boxcar smoothed by nine channels for clarity.

Here we will need the squint matrix for 3C 454.3, the equivalent of equation (15), which is

$$\begin{bmatrix} \tau'_{V,1} \\ V_{\mathrm{exp},1} \\ V_{\mathrm{sqnt,cos},1} \\ V_{\mathrm{sqnt,sin},1} \end{bmatrix} = \begin{bmatrix} 1.01 & -1.9\mathrm{E}-6\ \mathrm{K}^{-1} & -1.7\mathrm{E}-5\ \mathrm{K}^{-1} & -6.2\mathrm{E}-6\ \mathrm{K}^{-1} & +5.5\mathrm{E}-5\ \mathrm{K}^{-1} & +3.4\mathrm{E}-5\ \mathrm{K}^{-1} \\ 1.3\ \mathrm{K} & 1.01 & -0.01 & 0 & -1.42 & +0.14 \\ -5.4\ \mathrm{K} & +0.04 & 0.97 & +0.01 & -2.12 & +0.22 \\ +1.1\ \mathrm{K} & 0 & 0 & 1.00 & +0.02 & -0.67 \end{bmatrix} \times \begin{bmatrix} \tau'_{V,\mathrm{true}} \\ V_{\mathrm{exp},1} \\ V_{\mathrm{sqnt,cos,true}} \\ V_{\mathrm{sqnt,sin,true}} \\ V_{\mathrm{sqsh,cos,true}} \\ V_{\mathrm{sqsh,sin,true}} \end{bmatrix}. \tag{22}$$

Note, as anticipated in the discussion of equation (14), that the matrix elements on the first row tend to be inversely proportional to the source flux: 3C 454.3 is about 2.4 times more intense than 3C 138. Also, of course, the above 4×6 matrix elements for V are comparable to those for Q and U.

Figure 4 is the 3C 454.3 equivalent of 3C 138 (Fig. 3), in which the middle and bottom panels show the uncorrected $[\tau'_1(\nu)]$ and gain-corrected $[\Delta\tau'_1(\nu)]$ spectra, respectively. The spectra in the bottom panel should be zero. They are, in fact, zero except for bumps at the 5×10^{-4} level in both $\Delta\tau'_{Q,1}(\nu)$ and $\Delta\tau'_{U,1}(\nu)$ near VLSR $= -12$ and 0 km s^{-1}. These bumps must be the instrumental contribution from polarized sidelobes.

The polarized sidelobes produce this contribution according to the matrix elements of equation (22), which for the squintlike terms are about 1×10^{-5} K^{-1}. A bump of 5×10^{-4} in $\Delta\tau'_{U,1}(\nu)$ would need a combination of the cosine and sine components of either Q_{sqnt} or U_{sqnt} to be $\sim(5 \times 10^{-4})/\left(1 \times 10^{-5}\ \mathrm{K}^{-1}\right) = 50$ K. The actual values, not plotted here to save space and forestall the wrath of the Almighty, are $\sim$0.4 K. The bumps in $\Delta\tau'_1(\nu)$ cannot be from squintlike behavior.

Thus, for 3C 454.3 $\Delta\tau'_{Q,1}(\nu)$ and $\Delta\tau'_{U,1}(\nu)$ are nonzero while the true values should be zero. The 3C 454.3 bumps are about 3 times smaller than the 3C 138 ones, while 3C 454.3 has flux 2.4 times larger; thus, the ratios of the bump to the source flux are comparable. This is roughly what is expected if the bumps are caused by V_{sqnt} and V_{sqsh}, because the first-row matrix elements are roughly in the ratio of the source fluxes. We conclude that for both sources the production mechanism involves the polarized beam interacting with angular derivatives of H I emission. Moreover, there is no squintlike behavior in this interaction, because it has been fitted for and thereby automatically subtracted out.

6.3. *Possible Production Mechanisms for Fake Linear Polarization*

The unreal Stokes $[\Delta\tau_{Q,1}(\nu), \Delta\tau_{U,1}(\nu)]$ bumps we see in 3C 454.3 (and, probably, the bumps we see in 3C 138) cannot be from squintlike contributions, because these have been removed in the least-squares fit. There are three possible production mechanisms for these unreal bumps:

1. One is the semirandom components of the squintlike contributions (Q_{sqnt}, U_{sqnt}) (see item 2, § 4). From Heiles et al. (2001a), these are smaller than the uniform components of (Q_{sqnt}, U_{sqnt}). For 3C 454.3, we estimated the squint contribution to be small compared to the bumps. That the semirandom component of squint might be larger than the mean squint is not reasonable.
2. Another is the squashlike components. The larger of the two squashlike matrix elements in each of equations (15) and (22) are $\sim 5 \times 10^{-5}$ K^{-1}. The unreal $\sim$0.003 bumps in $\Delta\tau_1(\nu)$ for 3C 138 and the unreal 5×10^{-4} bumps for 3C 454.3 would need bumps in $Q_{\mathrm{sqsh,\,cos,\,true}}(\nu)$ of $\sim 0.003/(5 \times 10^{-5}\ \mathrm{K}^{-1}) = 60$ K and $\sim(5 \times 10^{-4})/(5 \times 10^{-5}\ \mathrm{K}^{-1}) = 10$ K, respectively. These are very much larger than the squintlike contributions—25 times larger for the case 3C 454.3. The possibility that squashlike contributions are this much larger than squint ones is unreasonable.
3. Finally, we have the far-out sidelobes, which are unmeasurable and unpredictable.

By eliminating the other possibilities, we conclude that for 3C 138 the observed fake linear polarization results from the polarized far-out sidelobes. This is the same conclusion we will reach in § 8.3 when discussing the empirical squintlike contribution to $V_{\mathrm{exp},0}(\nu)$.

7. AN ALTERNATIVE RECIPE FOR DETERMINING THE LEVEL OF INSTRUMENTAL EFFECTS IN $\tau_{V,2}(\nu)$

Our discussion in § 6 shows two things:

1. At Arecibo, polarized sidelobes outside the main beam and first sidelobe, together with angular structure in the sky, contribute importantly to the contribution to instrumental polarization;
2. The effect of polarized sidelobes is expected to be $\sim$10 times worse in linear than in circular polarization, i.e., in Stokes (Q, U) than in Stokes V.

This leads to use the following alternative recipe for determining the level of instrumental effects in $\tau_{V,2}(\nu)$.

First, least-squares fit the Stokes V spectra for squintlike and squashlike behavior to derive $\tau'_{V,2}(\nu)$. This eliminates not only the contribution from squint and squash proper (which, as defined in this paper, come from the main beam and first sidelobe), but also similar PA behavior arising from the far-out sidelobes. Similarly, we fit for squintlike behavior in Stokes (Q, U) to derive $\tau'_{Q,1}(\nu)$, $\tau'_{U,1}(\nu)$; we also gain-correct them to derive $\Delta\tau'_{Q,1}(\nu)$, $\Delta\tau'_{U,1}(\nu)$. For all three Stokes parameters, the least-squares fit leaves us with the PA-independent portions, which are the ones of interest.

Next, we expect the linear polarization to be zero, so we assume that any departures of $\Delta\tau'_{Q,1}(\nu)$, $\Delta\tau'_{U,1}(\nu)$ from zero are instrumental, the result of non-squintlike behavior of the far-out sidelobes. This is an upper limit because there might, in fact, be true linear polarization. At Arecibo beam effects in linear polarization are about 10 times those in circular polarization, so calculate the linear polarization $\tau'_{QU,1}(\nu) = [\Delta\tau'_{Q,1}(\nu)^2 + \Delta\tau'_{U,1}(\nu)^2]^{1/2}$ and divide it by 10 to estimate the remaining non-squintlike instrumental effects that remain in the $\tau'_{V,2}(\nu)$ spectrum.

In our plots of $\tau'_{V,2}$ we include this alternative estimate of the uncertainty, along with $\delta\tau'_{V,2}(\nu)$ as discussed in § 5.2.2.

8. SQUINT AND SQUASH CONTRIBUTIONS TO STOKES *V* EMISSION SPECTRA

The above sections concentrate on the uncertainties in the Stokes *V opacity* spectrum $\tau'_V(\nu)$ and its cousins $\tau'_Q(\nu)$ and $\tau'_U(\nu)$. In principle, we can also derive the circular polarization of the expected *emission* profile $V_{\rm exp}(\nu)$. Here we address the efficacy of doing this, i.e., we estimate squintlike and squashlike instrumental contributions to $V_{\rm exp}(\nu)$. We find that we cannot derive reliable values of $V_{\rm exp}(\nu)$, primarily because of our incomplete sampling of PA.

8.1. *Empirical Evaluation: the Example of 3C 138*

As with the polarized opacity spectra, we can derive the polarized emission spectra for the three cases discussed in § 5.1, namely ignoring squint and squash, removing squint only, and removing both squint and squash. Figure 5 exhibits these three versions $V_{\rm exp,0}(\nu)$, $V_{\rm exp,1}(\nu)$, and $V_{\rm exp,2}(\nu)$ for 3C 138. There are large differences between the three versions. The spectra change shape and become noisier as we work our way from $V_{\rm exp,0}(\nu)$ to $V_{\rm exp,2}(\nu)$. This occurs because of the covariance produced by incomplete PA coverage, as discussed in § 5. We cannot exclude the possibility that most of the contribution to $V_{\rm exp,0}(\nu)$ is from the squintlike and squashlike behaviors, i.e., the components of $V_{\rm sqnt,true}(\nu)$ and $V_{\rm sqsh,true}(\nu)$.

Figures 6 and 7 show the various measured (not the true) squintlike and squashlike contributions. These contribute to the various versions of $V_{\rm exp}(\nu)$ according to the relevant matrix elements in the second rows of equations (14), (15), and (16). As an example, for $V_{\rm exp,0}(\nu)$, which is derived including neither the squintlike nor squashlike PA dependence, the ($V_{\rm sqnt,cos,1}$, $V_{\rm sqnt,sin,1}$) components contribute by their values multiplied by the corresponding matrix elements in equation (14) (-0.29 and -0.21, respectively). These amount to a fake contributions to $V_{\rm exp,0}(\nu)$ of $\sim$0.04 K. This is comparable to the difference $[V_{\rm exp,0}(\nu) - V_{\rm exp,1}(\nu)]$.

For $V_{\rm exp,1}(\nu)$, derived including only the squintlike PA dependence, the matrix elements drop to less than 0.005 (denoted by "0" in eq. [15]), making the squintlike contribution negligible. One is tempted to think that the remaining 0.1 K level bumps in $V_{\rm exp,1}(\nu)$, shown in Figure 5, are real. However, the squashlike matrix element for $V_{\rm sqsh,cos,true}$ is huge, -1.33, so it is conceivable that the 0.1 K bumps are produced by squashlike behavior; alternatively, they might be produced by far-out sidelobes whose contribution is neither squintlike nor squashlike.

To elucidate these matters we compare the true squint/squash contributions, which come from only the main beam and first sidelobe, with the squintlike and squashlike contributions, which come from all parts of the telescope beam. First we evaluate the true contributions.

8.2. *Prediction of True Squint and Squash Contributions to Stokes V Spectra Using Angular Derivatives*

Here we discuss specifically only *true* squint and squash—namely, those portions of squintlike and squashlike behaviors that are produced by the primary beam and the first sidelobe. Heiles et al. (2001a) have evaluated the contribution to the Stokes *V* emission spectrum from true beam squint and true beam squash interacting with the first and second spatial derivatives of the spatially extended H I distribution. We use their formulation to predict this instrumental ("fake") contribution, which we denote with the subscript "fake." In their § 6 Heiles et al. (2001a) consult their Figure 14 to find that

$$|V_{\rm fake}| \lesssim \left|0.015\,\frac{dI}{d\theta}\right| + \left|0.025\,\frac{d^2I}{d\theta^2}\right|, \tag{23}$$

where I and V are antenna temperatures in K; θ is the angle in the sky, units are arcmin. The first term is squint, the second squash. The $\lesssim$ sign appears because (1) the equation is approximate; (2) it is an upper limit because it assumes that the absolute values of the contributions from the first and second spatial derivatives add arithmetically, while in fact they can cancel; and (3) the contributions of each term are periodic in PA or 2PA, so when observations are averaged over hour angle the instrumental contributions partially cancel.

Equation (23) provides the fake *V* emission spectrum for a particular position. We could pursue this for the opacity spectra, also. However, they are derived by ON–OFF observations—in fact, 16 of them—and the resulting instrumental contributions contain terms in $(d^3I/d\theta^3)\Delta\theta^2$ for squint and $(d^4I/d\theta^4)\Delta\theta^3$ for squash; here $\Delta\theta$ is the distance between ON and OFF measurements. We cannot evaluate these terms observationally, so it is not worth discussing opacity spectra.

8.3. *Comparison of Empirical and Predicted V Opacity Spectra for the Example of 3C 138*

We denote this predicted spectrum by $V_{\rm exp,fake}(\nu)$ and show it in Figure 8. There are two distinct parts, the squint (*dashed line*) and squash (*dash-dotted line*), from the first and second terms in equation (23), respectively; both are important. $V_{\rm exp,fake}(\nu)$ has a peak level $\sim$0.08 K. For comparison, the top panels of Figures 7 and 6 show the *empirically determined* $V_{\rm sqnt,sin,1}(\nu)$ and $V_{\rm sqnt,cos,1}(\nu)$. They have peak levels $\sim$0.15 K. This is about 4 times larger than the peak predicted squint. The ratio for some other sources is larger; for example, for 3C 207 the ratio is about 8. Likewise, the empirically determined squashlike contributions in Figures 6 and 7 (*bottom panels*) have peak values $\sim$0.2 K, about 4–5 times larger than the peak predicted squash in Figure 8.

We conclude that the empirically determined squintlike and squashlike contributions are considerably larger than the true squint and squash expected from the main beam and first sidelobe. The empirically determined ones include not only the true squint and

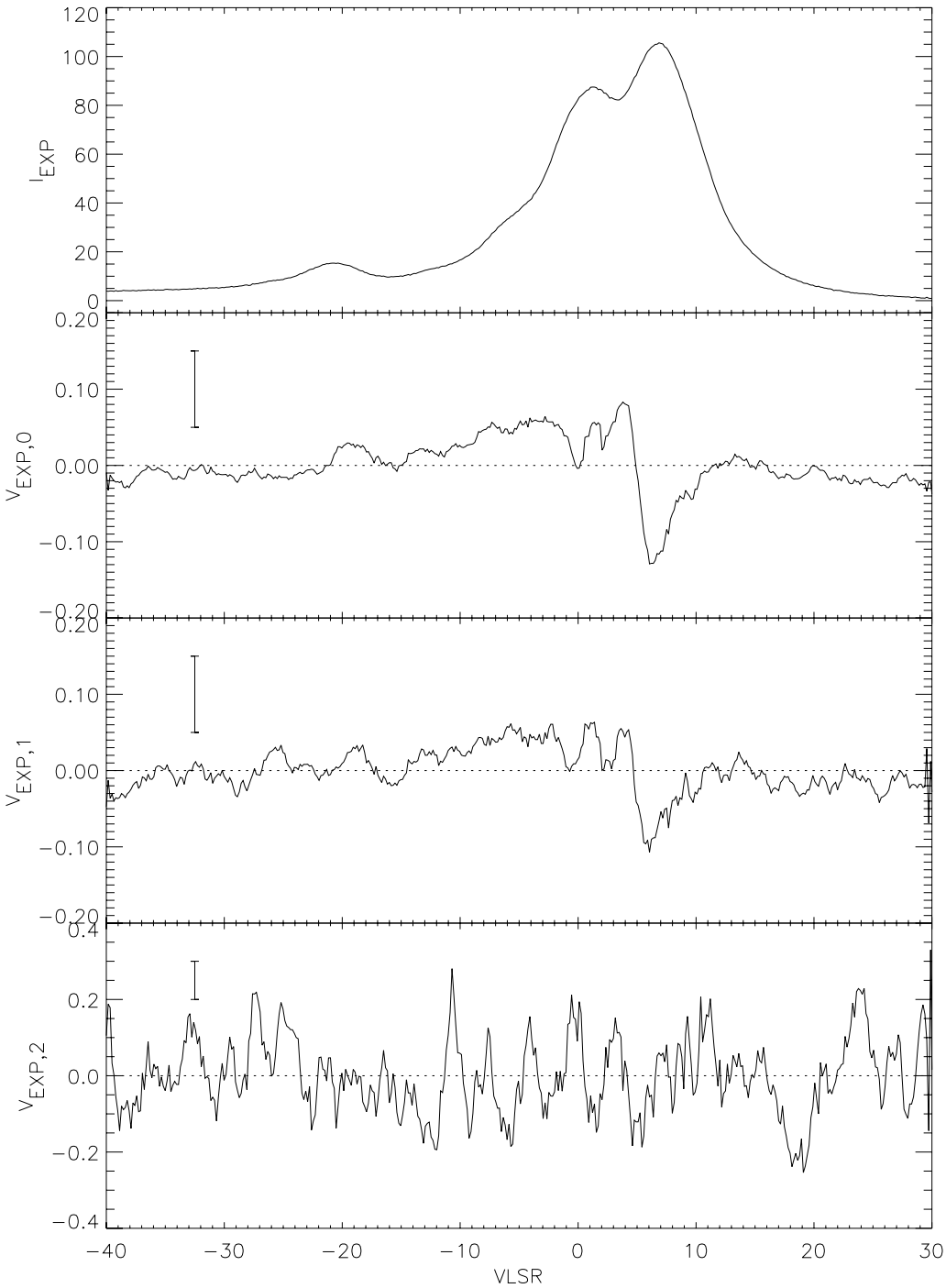

FIG. 5.—3C 138 expected emission profile analog of the opacity spectra in Fig. 2. The top panel is the expected Stokes I emission profile $I_{\rm exp}(\nu)$ (twice the conventionally defined brightness temperature). The second panel is $V_{\rm exp,0}(\nu)$, derived by ignoring squint and squash; the third is $V_{\rm exp,1}(\nu)$, derived by including squint but not squash in the fit; and the fourth is $V_{\rm exp,2}(\nu)$, derived by including both squint and squash. The bottom three are gain-corrected and boxcar-smoothed by nine channels for clarity. As shown by the sample error bar, the vertical scale on the bottom panel is 2 times larger than on the second and third panels.

squash, but also the contribution from far-out sidelobes. We conclude that the far-out sidelobes dominate the contribution to the observed squint and squash.

Even weak far-out sidelobes can produce these effects. They span large angles in the sky. Over these large angles, the H I angular structure can change considerably; this exaggerates the contribution of these sidelobes. As a specific example, Heiles et al. (2001a) find that the first sidelobe's contribution to $V_{\rm sqnt,1}$ is almost twice that of the main beam, while its contribution to I is only $\sim\frac{1}{3}$ that of the main beam.

We eliminate the squintlike contribution to $V_{\rm exp}(\nu)$ by including it in the least-squares fit. However, we cannot eliminate the squashlike component by fitting because of the noise, which results from the covariance. To obtain accurate results, these instrumental contributions must be removed with high reliability. This might be possible by fitting for the squash, as in $V_{\rm exp,1}(\nu)$, but the excess noise produced by the covariance is prohibitive. We conclude that we cannot derive $V_{\rm exp}(\nu)$ for 3C 138.

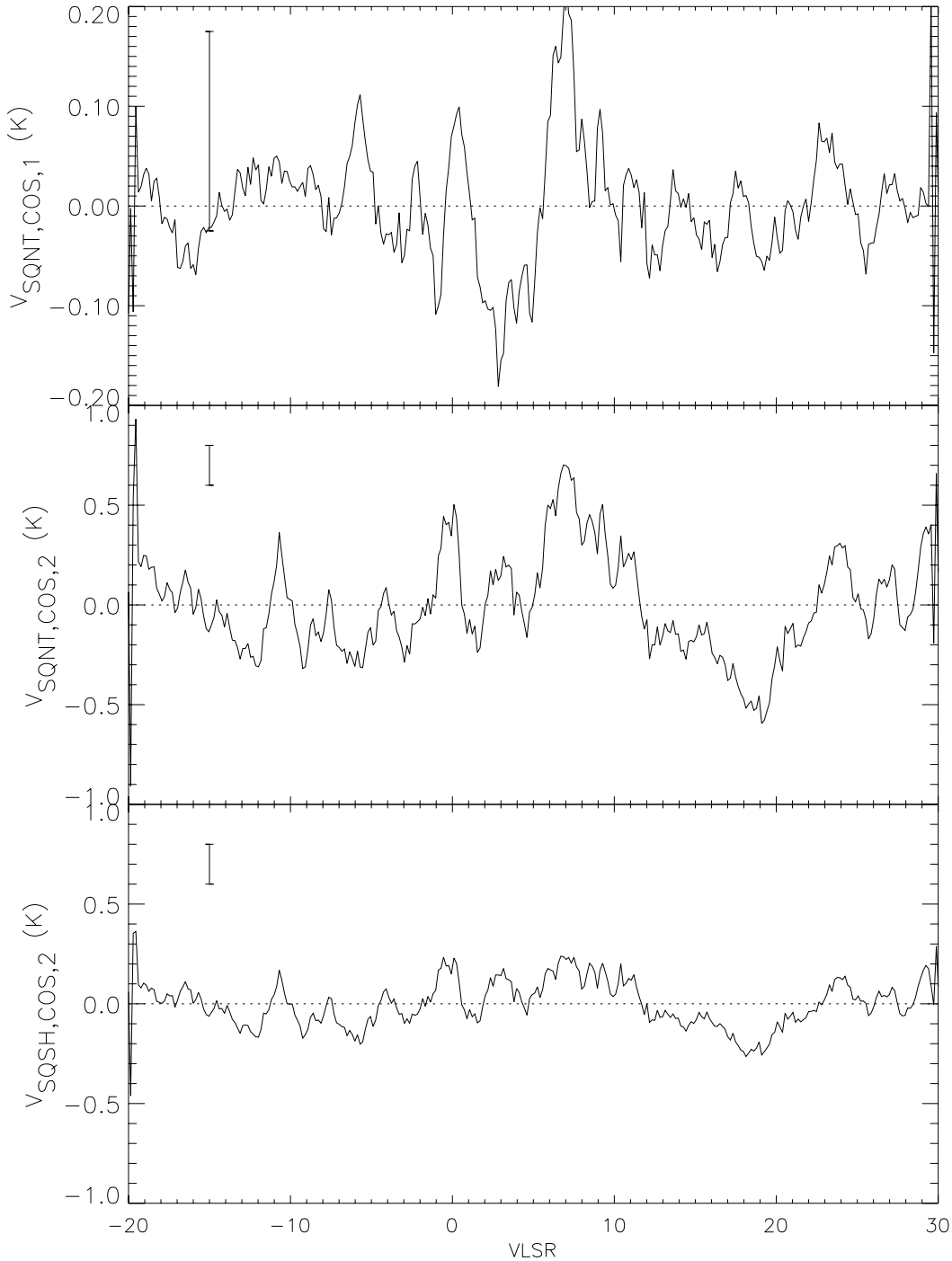

FIG. 6.—Cosine components $V_{\rm sqnt,cos}(\nu)$ and $V_{\rm sqsh,cos}(\nu)$ for 3C 138. The first (*top*) panel exhibits $V_{\rm sqnt,cos,1}$, derived by solving eq. (10d) including only the squintlike terms in eqs. (13a)–(13b). The second and third exhibit $V_{\rm sqnt,cos,2}$ and $V_{\rm sqsh,cos,2}$ derived by including both squintlike and squashlike terms. As shown by the sample error bar, the vertical scales of the two lower panels are 5 times that of the top panel. All spectra are boxcar smoothed by nine channels to reduce the noise.

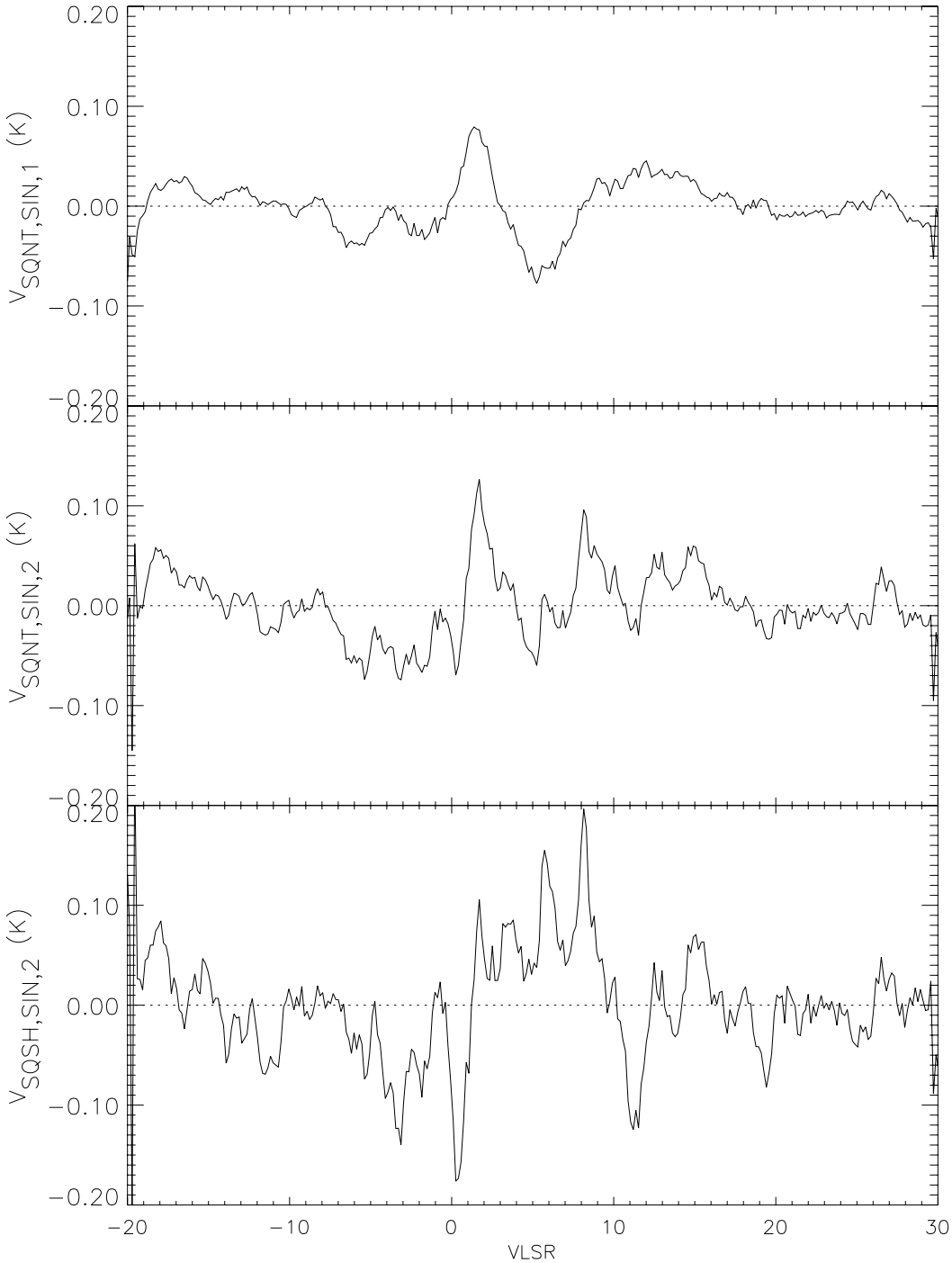

FIG. 7.—Sine components $V_{\mathrm{sqnt,sin}}(\nu)$ and $V_{\mathrm{sqsh,sin}}(\nu)$ for 3C 138. The first (*top*) panel exhibits $V_{\mathrm{sqnt,sin,1}}$, derived by solving eq. (10d) including only the squintlike terms in eqs. (13a)–(13b). The second and third exhibit $V_{\mathrm{sqnt,sin,2}}$ and $V_{\mathrm{sqsh,sin,2}}$ derived by including both squintlike and squashlike terms. All spectra are boxcar smoothed by nine channels to reduce the noise.

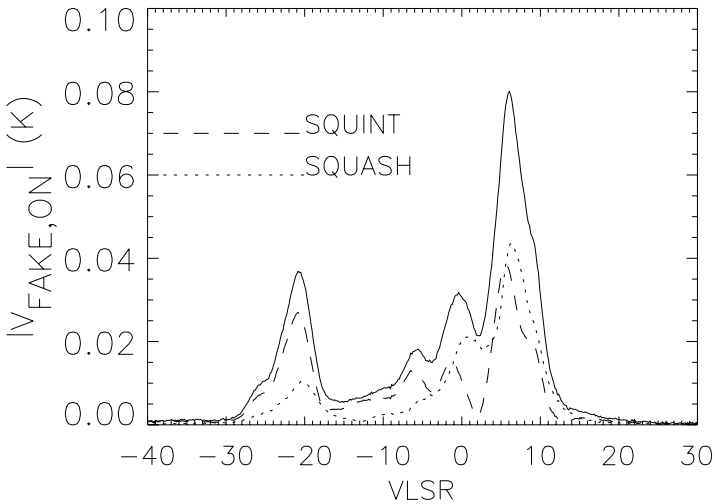

FIG. 8.—Instrumental ("fake") on-source emission V profile $|V_{\rm fake,on}(\nu)|$, from eq. (23). This is the contribution from true squint and squash, i.e., from the primary beam and first sidelobe only.

Unfortunately, none of our sources exhibits a believable $V_{\rm exp,1}(\nu)$ profile. In some cases, such as 3C 123, $V_{\rm exp,0}(\nu)$ suggests a Zeeman-splitting signal but we have insufficient PA coverage to determine even the squintlike component. We were not always able to obtain good PA coverage because of practical considerations regarding the telescope schedule and our source list. In other cases, such as 3C 138, the squintlike and/or squashlike component is disturbingly large. Telescopes with fewer far-out sidelobes than Arecibo are desirable, and perhaps even necessary, to determine reliable Zeeman splitting of emission profiles.

8.4. *Regarding Magnetic Fields*

A magnetic field of $B_\parallel$ μG produces Zeeman splitting $\delta\nu_Z = 2.8B_\parallel$ Hz, which produces $V_Z(\nu) \sim (2.8B_\parallel/\Delta\nu_{\rm FWHM})I(\nu)$, where $\Delta\nu_{\rm FWHM}$ is the half-power line width. For a line of width 2 km s^{-1}, we have the uncertainty in magnetic field $\Delta B_\parallel \sim 3000[V(\nu)/I(\nu)]$. For 3C 138 we have the peak $I(\nu) \sim 100$ K and the uncertainty in $V_{\rm exp}(\nu) \sim 0.2$ K, so the uncertainty in fractional circular polarization is $\sim$0.002. This gives $\Delta B_\parallel \sim 6$ μG, which is unacceptably large. We conclude that use of our data for determining $V_{\rm exp,1}(\nu)$, i.e., the circular polarization of *emission* profiles, at the levels required for determining magnetic fields is unwarranted unless the actual magnetic fields are very high or instrumental effects happen to be unusually small.

9. RESULTS

9.1. *Graphical Results*

Our Paper I/Paper II survey covered 79 continuum sources. Of these, 61 had detectable CNM. Of these, we had enough integration time for Zeeman-splitting measurements on 39. Here we add two additional sources, Tau A (observed at Arecibo) and Cas A (observed years ago at HCRO). Therefore, we have a total of 41 sources.

Figure 9*a* presents the data for 3C 138 in three panels. The top panel exhibits $\tau_0(\nu)$ as the large black dotted line, together with the fitted Gaussians from Paper I as the light dotted lines. This panel is annotated with information about the Gaussians. The middle panel shows $\tau_2'(\nu)$ as the solid line, and the least-squares fit to $B_\parallel$ as the dashed line; the fitted field for each Gaussian is different, and the values are shown in the annotations of the top panel. The bottom panel provides information on possible instrumental contributions: the top solid line is the expected instrumental contribution $\delta\tau_2'(\nu)$ from equation (17), and the bottom solid line shows one-tenth the linearly polarized profile $\tau_{QU,1}'(\nu)/10$ as described in § 7. We provide plots equivalent to Figure 9 for all sources in the electronic edition of *The Astrophysical Journal Supplement*.

9.2. *Tabular Results for Gaussian Components*

Typically, each source has several CNM components, which we represent by Gaussians as described in Paper I. Our 41 sources have a total of 151 components. However, some of these have such large errors in the derived $B_\parallel$ that they are not worth considering. Table 1 lists all Gaussian components for which $\Delta B < 100$ μG; these number 136.

If we define a "detection" as $|B_\parallel| > 2.5\Delta B_\parallel$, where $\Delta B_\parallel$ is the 1 σ uncertainty, and in addition if we require $\Delta B_\parallel < 10$ μG, then we have 69 components and 22 detections; including results with $\Delta B_\parallel < 10$ μG brings the 22 up to 26, but we discount these (see below). If we were to restrict our discussion to the 22 sure detections, there is little we could say except to comment on individual sources. However, if we include the ensemble of results and discuss them statistically, we can do much more.

Our results on $B_\parallel$ are unique among H I Zeeman-splitting work in that the errors $\Delta B_\parallel$ should be reasonably free of instrumental contributions, as shown by our discussion in the above sections. This low instrumental contribution occurs because H I absorption lines are the results of ON-OFF measurements, which switches out most of the instrumental contribution. In contrast, other large Zeeman-splitting surveys (e.g., Heiles 1989) examine the H I line in emission; these are ON measurements, and the instrumental contribution is a nontrivial portion of the measured results (Heiles 1996). With our current absorption line measurements, there is no

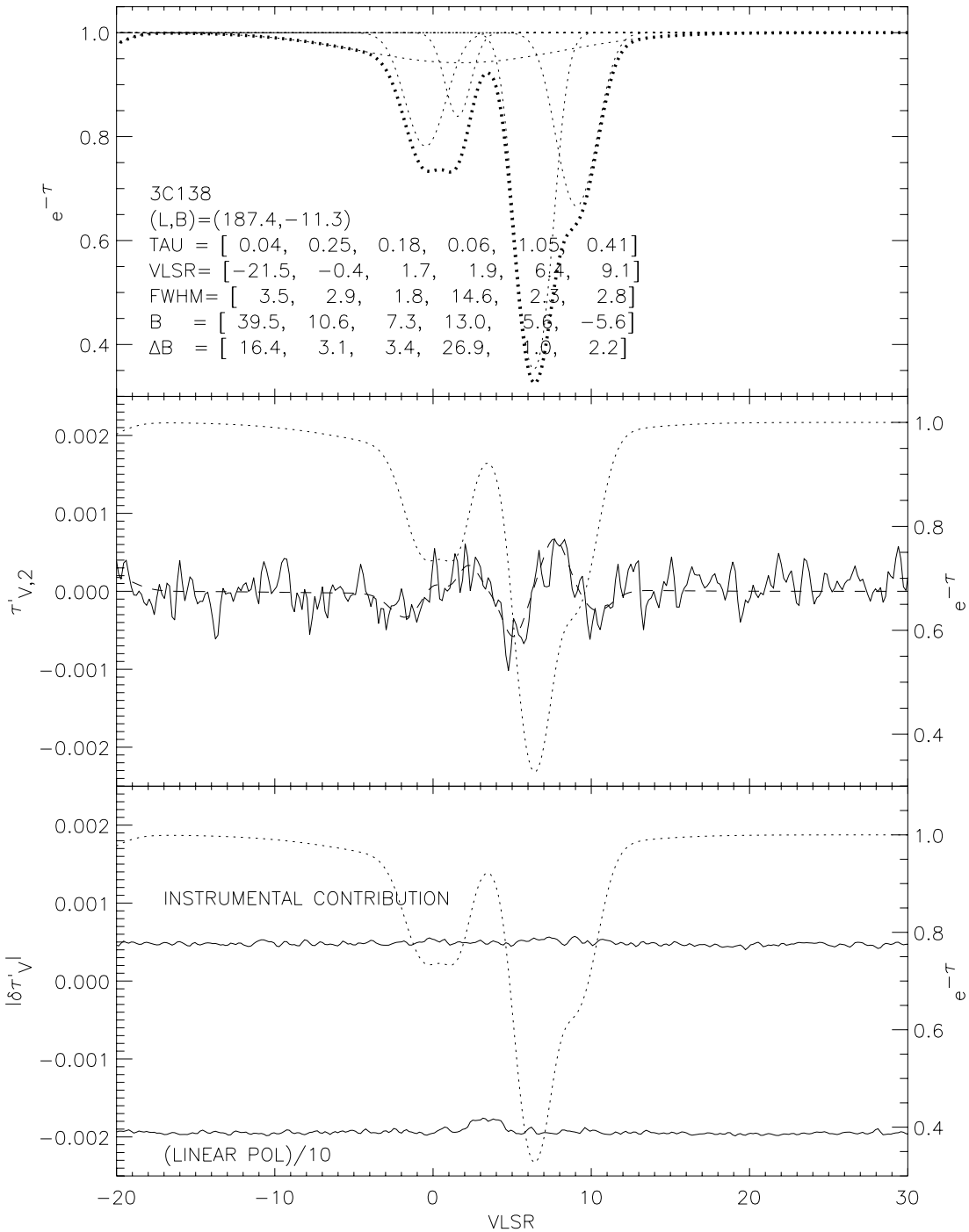

FIG. 9.—Derived spectra for 3C 138; plots for all sources are available in the electronic edition of *The Astrophysical Journal*. The top panel exhibits $\tau_0(\nu)$ as the large black dotted line, together with the fitted Gaussians from Paper I as the light dotted lines. This panel is annotated with information about the Gaussians. The middle panel shows $\tau_2'(\nu)$ as the solid line and the least-squares fit as the dashed line. The bottom panel provides information on possible instrumental contributions as described in the text.

TABLE 1

Table of Gaussian Fit Parameters Having $\Delta B_{\|} < 100\ \mu$G

T_B	τ	$V_{\rm LSR}$	ΔV	T_s	$T_{\rm kmax}$	N(H I)$_{20}$	$B_{\|}$	(l/b/Source)
34.34.....	1.666 ± 0.007	7.6 ± 0.0	4.48 ± 0.01	42.34 ± 9.96	438	6.15	−1.6 ± 1.9	190.4/−27.4/3C 120
19.32.....	0.736 ± 0.010	6.2 ± 0.0	1.33 ± 0.02	37.08 ± 6.86	38	0.71	5.2 ± 3.8	190.4/−27.4/3C 120
20.65.....	0.634 ± 0.008	10.2 ± 0.0	1.91 ± 0.02	43.96 ± 3.95	79	1.04	3.6 ± 2.8	190.4/−27.4/3C 120
80.96.....	0.596 ± 0.026	4.7 ± 0.0	2.32 ± 0.08	180.36 ± 115.21	117	4.86	4.8 ± 4.2	170.6/−11.7/3C 123
13.50.....	1.606 ± 0.026	4.4 ± 0.0	4.79 ± 0.02	16.88 ± 7.44	501	2.53	−2.6 ± 1.0	170.6/−11.7/3C 123
2.51.....	0.063 ± 0.002	−19.6 ± 0.0	3.14 ± 0.11	40.93 ± 6.20	215	0.16	1.2 ± 8.6	170.6/−11.7/3C 123
0.18.....	0.008 ± 0.001	−57.8 ± 0.5	5.62 ± 1.09	22.15 ± 40.62	691	0.02	−11.4 ± 86.9	170.6/−11.7/3C 123
0.57.....	0.032 ± 0.002	−72.9 ± 0.1	4.28 ± 0.24	17.79 ± 10.26	400	0.05	−4.7 ± 19.3	170.6/−11.7/3C 123
0.00.....	0.007 ± 0.002	20.0 ± 0.5	3.88 ± 1.09	0.00 ± 0.00	328	0.00	55.1 ± 86.1	170.6/−11.7/3C 123
39.30.....	2.152 ± 0.034	5.3 ± 0.0	4.24 ± 0.04	44.47 ± 8.06	392	7.90	0.7 ± 8.4	171.4/−7.8/3C 131
21.36.....	0.321 ± 0.006	−2.3 ± 0.1	6.95 ± 0.21	77.79 ± 5.43	1057	3.38	2.8 ± 36.2	171.4/−7.8/3C 131
19.68.....	0.260 ± 0.006	13.0 ± 0.1	5.68 ± 0.23	85.86 ± 9.64	705	2.47	9.7 ± 5.5	178.9/−12.5/3C 132
43.75.....	1.542 ± 0.028	8.1 ± 0.0	2.42 ± 0.03	55.66 ± 14.67	128	4.05	4.2 ± 1.0	178.9/−12.5/3C 132
9.04.....	0.351 ± 0.007	1.8 ± 0.1	5.43 ± 0.12	30.52 ± 11.08	643	1.13	−4.0 ± 3.8	178.9/−12.5/3C 132
30.18.....	1.532 ± 0.021	8.0 ± 0.0	2.51 ± 0.02	38.50 ± 13.68	138	2.89	5.8 ± 1.1	177.7/−9.9/3C 133
25.98.....	0.891 ± 0.021	3.7 ± 0.0	2.77 ± 0.06	44.04 ± 17.06	167	2.12	−0.3 ± 1.7	177.7/−9.9/3C 133
15.35.....	0.262 ± 0.006	−0.2 ± 0.2	6.17 ± 0.31	66.60 ± 11.51	831	2.10	−9.5 ± 6.3	177.7/−9.9/3C 133
1.16.....	0.064 ± 0.009	−27.6 ± 0.2	2.84 ± 0.46	18.79 ± 6.96	176	0.07	15.1 ± 14.2	177.7/−9.9/3C 133
12.83.....	0.060 ± 0.008	−29.5 ± 0.4	8.45 ± 0.63	219.27 ± 5.45	1559	2.17	−41.8 ± 25.0	177.7/−9.9/3C 133
25.99.....	1.046 ± 0.008	6.4 ± 0.0	2.30 ± 0.02	40.07 ± 12.30	115	1.87	5.6 ± 1.0	187.4/−11.3/3C 138
15.70.....	0.406 ± 0.005	9.1 ± 0.0	2.81 ± 0.06	47.02 ± 11.54	172	1.05	−5.6 ± 2.2	187.4/−11.3/3C 138
8.48.....	0.176 ± 0.014	1.6 ± 0.1	1.84 ± 0.09	52.62 ± 11.03	73	0.33	7.3 ± 3.4	187.4/−11.3/3C 138
11.82.....	0.247 ± 0.006	−0.5 ± 0.1	2.86 ± 0.12	54.03 ± 9.60	178	0.74	10.6 ± 3.1	187.4/−11.3/3C 138
21.94.....	0.060 ± 0.004	1.8 ± 0.2	14.64 ± 0.48	379.12 ± 23.44	4683	6.44	13.0 ± 26.9	187.4/−11.3/3C 138
3.78.....	0.038 ± 0.002	−21.5 ± 0.1	3.45 ± 0.21	101.52 ± 5.08	260	0.26	39.5 ± 16.4	187.4/−11.3/3C 138
44.11.....	2.362 ± 0.045	7.0 ± 0.0	3.13 ± 0.03	48.69 ± 15.55	214	7.02	−8.3 ± 1.3	197.6/−14.5/3C 142.1
4.22.....	0.203 ± 0.007	13.4 ± 0.1	4.12 ± 0.17	23.03 ± 10.75	370	0.37	7.2 ± 7.4	197.6/−14.5/3C 142.1
9.51.....	0.083 ± 0.007	22.4 ± 0.1	3.39 ± 0.32	119.08 ± 10.47	251	0.65	−23.3 ± 14.9	197.6/−14.5/3C 142.1
0.90.....	0.101 ± 0.007	−9.2 ± 0.1	3.24 ± 0.26	9.37 ± 13.82	229	0.06	0.8 ± 12.1	197.6/−14.5/3C 142.1
30.83.....	0.919 ± 0.014	1.8 ± 0.0	2.63 ± 0.07	51.28 ± 18.44	151	2.42	−9.8 ± 1.7	185.6/4.0/3C 154
6.05.....	0.292 ± 0.019	−2.1 ± 0.0	1.32 ± 0.10	23.87 ± 18.23	37	0.18	−6.0 ± 4.0	185.6/4.0/3C 154
24.81.....	0.709 ± 0.014	−2.9 ± 0.0	4.45 ± 0.06	48.85 ± 14.40	433	3.01	−5.1 ± 2.4	185.6/4.0/3C 154
19.70.....	0.479 ± 0.007	5.0 ± 0.1	3.48 ± 0.10	51.78 ± 15.58	263	1.68	−6.3 ± 2.8	185.6/4.0/3C 154
10.83.....	0.413 ± 0.006	10.6 ± 0.0	2.12 ± 0.03	31.98 ± 9.17	98	0.55	0.1 ± 2.0	185.6/4.0/3C 154
11.61.....	0.068 ± 0.003	−23.7 ± 0.1	4.35 ± 0.22	176.60 ± 5.51	412	1.02	−3.9 ± 14.3	185.6/4.0/3C 154
38.18.....	0.252 ± 0.008	22.6 ± 0.4	21.71 ± 0.98	171.23 ± 6.90	10301	18.26	−40.5 ± 33.1	207.3/1.2/3C 167
50.50.....	0.941 ± 0.024	42.2 ± 0.1	8.01 ± 0.23	82.85 ± 12.73	1403	12.16	39.2 ± 7.7	207.3/1.2/3C 167
8.60.....	0.386 ± 0.032	49.3 ± 0.1	2.09 ± 0.19	26.87 ± 5.61	95	0.42	−24.6 ± 7.6	207.3/1.2/3C 167
16.71.....	0.669 ± 0.011	−8.9 ± 0.0	2.43 ± 0.03	34.25 ± 7.89	129	1.09	−1.2 ± 1.5	118.6/−52.7/3C 18
8.15.....	0.183 ± 0.018	−5.7 ± 0.1	3.99 ± 0.25	48.75 ± 9.41	347	0.69	12.8 ± 7.0	118.6/−52.7/3C 18
19.42.....	0.075 ± 0.019	−6.7 ± 0.2	8.68 ± 0.70	267.80 ± 5.28	1648	3.41	26.5 ± 21.6	118.6/−52.7/3C 18
5.39.....	0.068 ± 0.002	8.0 ± 0.1	4.30 ± 0.12	82.14 ± 3.76	403	0.47	−28.1 ± 12.0	197.9/26.4/3C 192
5.03.....	0.298 ± 0.004	15.4 ± 0.0	2.43 ± 0.03	19.53 ± 2.66	129	0.28	−1.9 ± 2.2	213.0/30.1/3C 207
5.46.....	0.250 ± 0.002	4.2 ± 0.0	5.25 ± 0.05	24.65 ± 4.74	602	0.63	−3.2 ± 3.7	213.0/30.1/3C 207
5.78.....	0.313 ± 0.003	4.0 ± 0.0	1.32 ± 0.01	21.53 ± 1.30	37	0.17	−1.2 ± 4.9	219.9/44.0/3C 225a
9.17.....	0.745 ± 0.002	3.6 ± 0.0	1.25 ± 0.00	17.44 ± 1.80	34	0.32	−1.3 ± 1.1	220.0/44.0/3C 225b
1.21.....	0.027 ± 0.001	−28.0 ± 0.1	4.78 ± 0.13	45.40 ± 3.28	499	0.11	3.6 ± 43.4	220.0/44.0/3C 225b
2.79.....	0.047 ± 0.001	−37.9 ± 0.1	2.52 ± 0.11	61.11 ± 1.97	138	0.14	−15.7 ± 20.2	220.0/44.0/3C 225b
0.53.....	0.033 ± 0.001	−40.6 ± 0.1	2.07 ± 0.12	16.64 ± 3.05	93	0.02	1.8 ± 26.1	220.0/44.0/3C 225b
4.47.....	0.398 ± 0.001	1.9 ± 0.0	1.19 ± 0.00	13.61 ± 0.26	31	0.13	−0.7 ± 1.1	232.1/46.6/3C 237
1.39.....	0.005 ± 0.000	−3.0 ± 0.1	2.48 ± 0.16	255.60 ± 10.79	134	0.07	45.6 ± 92.9	232.1/46.6/3C 237
0.81.....	0.018 ± 0.000	−6.3 ± 0.0	2.37 ± 0.04	44.43 ± 3.19	122	0.04	−29.6 ± 24.6	289.9/64.4/3C 273
3.80.....	0.102 ± 0.001	−1.6 ± 0.0	2.94 ± 0.04	39.15 ± 2.41	189	0.23	44.9 ± 13.1	269.9/83.2/3C 274.1
17.93.....	0.620 ± 0.003	−3.7 ± 0.0	1.75 ± 0.01	38.81 ± 3.37	66	0.82	−2.7 ± 1.3	38.5/60.2/3C 310
2.86.....	0.061 ± 0.001	0.6 ± 0.1	5.11 ± 0.13	48.36 ± 4.76	571	0.29	9.2 ± 17.8	38.5/60.2/3C 310
24.03.....	0.784 ± 0.011	−4.2 ± 0.0	2.15 ± 0.02	44.23 ± 2.20	100	1.45	−0.1 ± 1.1	39.3/58.5/3C 315
8.30.....	0.146 ± 0.004	1.6 ± 0.1	4.41 ± 0.15	61.00 ± 15.11	425	0.77	3.9 ± 6.3	39.3/58.5/3C 315
13.05.....	0.482 ± 0.013	−6.0 ± 0.0	1.77 ± 0.03	34.12 ± 4.47	68	0.57	−0.2 ± 4.1	30.0/54.8/3C 318
15.55.....	0.300 ± 0.011	−5.0 ± 0.0	3.36 ± 0.04	60.07 ± 5.81	246	1.18	−4.6 ± 7.6	30.0/54.8/3C 318
17.01.....	0.993 ± 0.010	0.9 ± 0.0	2.11 ± 0.02	27.01 ± 7.96	97	1.10	3.0 ± 1.7	37.6/42.3/3C 333
9.35.....	0.025 ± 0.000	−4.3 ± 0.0	8.91 ± 0.10	379.10 ± 3.26	1733	1.64	−30.9 ± 42.9	129.4/−49.3/3C 33
2.66.....	0.259 ± 0.003	−2.2 ± 0.0	1.65 ± 0.03	11.65 ± 4.80	59	0.10	1.4 ± 1.5	23.0/29.2/3C 348
14.76.....	0.604 ± 0.004	0.5 ± 0.0	2.12 ± 0.01	32.54 ± 5.82	98	0.81	0.0 ± 0.9	23.0/29.2/3C 348
8.53.....	0.078 ± 0.002	7.2 ± 0.0	3.73 ± 0.09	113.21 ± 1.57	304	0.64	0.5 ± 6.4	23.0/29.2/3C 348
25.87.....	1.209 ± 0.007	0.0 ± 0.0	2.80 ± 0.01	36.89 ± 10.12	170	2.43	4.2 ± 2.0	21.1/19.9/3C 353

TABLE 1—*Continued*

T_B	τ	V_{LSR}	ΔV	T_s	T_{kmax}	$N(\mathrm{H\ I})_{20}$	$B_{\parallel}$	(l/b/Source)
15.37.....	0.859 ± 0.006	2.4 ± 0.0	1.69 ± 0.01	26.66 ± 13.08	62	0.76	5.1 ± 2.0	21.1/19.9/3C 353
28.62.....	0.195 ± 0.008	1.4 ± 0.0	5.84 ± 0.07	161.35 ± 4.53	746	3.59	0.6 ± 11.8	21.1/19.9/3C 353
1.57.....	0.040 ± 0.001	11.9 ± 0.0	3.01 ± 0.07	39.89 ± 5.32	198	0.09	−15.7 ± 21.5	21.1/19.9/3C 353
11.93.....	0.451 ± 0.002	3.9 ± 0.0	3.03 ± 0.02	32.85 ± 7.01	201	0.88	3.3 ± 1.2	63.3/−5.9/3C 409
11.86.....	0.331 ± 0.003	7.7 ± 0.0	2.91 ± 0.04	42.08 ± 10.70	184	0.79	3.0 ± 1.7	63.3/−5.9/3C 409
20.64.....	0.753 ± 0.009	15.7 ± 0.0	1.69 ± 0.02	38.99 ± 13.10	62	0.97	5.4 ± 1.0	63.3/−5.9/3C 409
22.40.....	0.861 ± 0.010	13.7 ± 0.0	1.96 ± 0.02	38.80 ± 18.47	83	1.28	0.6 ± 1.0	63.3/−5.9/3C 409
10.44.....	0.413 ± 0.011	14.0 ± 0.0	6.90 ± 0.13	30.85 ± 11.38	1040	1.71	3.2 ± 2.5	63.3/−5.9/3C 409
5.17.....	0.035 ± 0.001	23.3 ± 0.1	4.27 ± 0.20	148.28 ± 13.67	399	0.44	−1.1 ± 13.7	63.3/−5.9/3C 409
52.84.....	2.214 ± 0.030	7.8 ± 0.0	2.77 ± 0.05	59.33 ± 24.84	167	7.08	1.4 ± 1.0	69.2/−3.8/3C 410
31.74.....	0.688 ± 0.009	11.3 ± 0.1	3.55 ± 0.11	63.79 ± 22.10	276	3.04	0.2 ± 2.1	69.2/−3.8/3C 410
13.06.....	0.369 ± 0.061	−0.7 ± 0.2	3.51 ± 0.21	42.30 ± 13.68	269	1.07	4.4 ± 3.0	69.2/−3.8/3C 410
26.67.....	0.654 ± 0.025	2.6 ± 0.2	4.33 ± 0.34	55.56 ± 22.19	409	3.06	5.2 ± 2.3	69.2/−3.8/3C 410
0.00.....	0.118 ± 0.004	17.8 ± 0.1	4.81 ± 0.25	0.00 ± 0.00	506	0.00	18.4 ± 8.3	69.2/−3.8/3C 410
8.04.....	0.103 ± 0.004	25.0 ± 0.1	3.54 ± 0.17	82.37 ± 8.82	274	0.58	7.9 ± 7.6	69.2/−3.8/3C 410
8.43.....	0.042 ± 0.004	−23.2 ± 0.2	3.52 ± 0.37	205.53 ± 15.95	270	0.59	12.5 ± 17.9	69.2/−3.8/3C 410
0.30.....	0.019 ± 0.005	−46.3 ± 0.3	2.53 ± 0.68	16.11 ± 29.14	139	0.02	11.2 ± 32.9	69.2/−3.8/3C 410
2.66.....	0.162 ± 0.008	2.1 ± 0.0	1.45 ± 0.06	17.85 ± 10.98	45	0.08	−0.7 ± 3.8	74.5/−17.7/3C 433
24.25.....	0.258 ± 0.007	3.0 ± 0.0	4.12 ± 0.09	106.60 ± 4.40	371	2.21	−0.6 ± 3.3	74.5/−17.7/3C 433
6.71.....	0.076 ± 0.003	6.9 ± 0.0	1.97 ± 0.10	92.22 ± 5.03	84	0.27	6.7 ± 6.6	74.5/−17.7/3C 433
4.39.....	0.053 ± 0.002	16.0 ± 0.0	3.11 ± 0.11	85.00 ± 4.10	210	0.27	14.7 ± 10.8	74.5/−17.7/3C 433
5.91.....	0.093 ± 0.001	3.9 ± 0.0	3.12 ± 0.05	66.22 ± 2.48	213	0.38	−0.3 ± 21.2	88.1/−35.9/3C 454.0
6.81.....	0.045 ± 0.001	−1.5 ± 0.1	6.39 ± 0.20	156.34 ± 5.71	892	0.87	−23.1 ± 62.3	88.1/−35.9/3C 454.0
7.59.....	0.091 ± 0.001	−2.0 ± 0.0	3.69 ± 0.07	86.97 ± 5.18	297	0.57	6.6 ± 3.6	86.0/−38.1/3C 454.3
3.50.....	0.079 ± 0.003	0.7 ± 0.0	1.81 ± 0.06	46.32 ± 4.91	71	0.13	3.4 ± 2.9	86.0/−38.1/3C 454.3
0.88.....	0.022 ± 0.001	3.4 ± 0.2	4.20 ± 0.35	40.89 ± 12.03	386	0.07	5.6 ± 15.5	86.0/−38.1/3C 454.3
10.73.....	0.298 ± 0.001	−10.1 ± 0.0	2.65 ± 0.01	41.65 ± 1.52	153	0.64	−2.1 ± 0.9	86.0/−38.1/3C 454.3
0.42.....	0.048 ± 0.001	−30.4 ± 0.0	2.00 ± 0.05	8.92 ± 3.30	87	0.02	0.8 ± 4.4	86.0/−38.1/3C 454.3
0.91.....	0.016 ± 0.001	−35.4 ± 0.1	3.36 ± 0.18	56.79 ± 7.80	246	0.06	−1.7 ± 16.5	86.0/−38.1/3C 454.3
2.18.....	0.015 ± 0.001	−16.8 ± 0.1	5.51 ± 0.27	151.25 ± 9.11	664	0.24	−51.7 ± 23.7	86.0/−38.1/3C 454.3
22.55.....	0.290 ± 0.007	−10.8 ± 0.1	5.10 ± 0.13	89.70 ± 4.14	569	2.58	30.3 ± 12.4	157.8/−48.2/3C 64
3.71.....	0.086 ± 0.007	0.2 ± 0.2	4.37 ± 0.38	45.23 ± 5.28	417	0.33	−16.7 ± 34.8	157.8/−48.2/3C 64
17.93.....	0.682 ± 0.006	−10.4 ± 0.0	2.32 ± 0.02	36.26 ± 4.06	117	1.12	5.0 ± 1.5	170.3/−44.9/3C 75
3.33.....	0.095 ± 0.004	−5.8 ± 0.1	2.74 ± 0.12	36.89 ± 3.43	163	0.19	−16.2 ± 8.8	170.3/−44.9/3C 75
11.02.....	0.113 ± 0.003	5.3 ± 0.1	5.19 ± 0.13	103.57 ± 6.97	589	1.18	−1.2 ± 10.2	170.3/−44.9/3C 75
28.24.....	1.108 ± 0.004	6.8 ± 0.0	2.24 ± 0.01	42.17 ± 7.17	109	2.04	−4.6 ± 1.0	174.9/−44.5/3C 78
4.29.....	0.082 ± 0.001	10.7 ± 0.1	4.26 ± 0.14	54.38 ± 6.31	396	0.37	19.9 ± 11.7	174.9/−44.5/3C 78
6.81.....	0.153 ± 0.002	4.2 ± 0.0	1.92 ± 0.05	47.89 ± 4.61	80	0.27	2.8 ± 4.5	174.9/−44.5/3C 78
6.81.....	0.116 ± 0.002	−7.7 ± 0.0	3.07 ± 0.06	62.07 ± 5.14	206	0.43	−14.3 ± 6.6	174.9/−44.5/3C 78
7.09.....	0.297 ± 0.017	9.5 ± 0.0	1.35 ± 0.09	27.59 ± 20.46	39	0.21	−2.8 ± 4.8	179.8/−31.0/3C 98
38.72.....	0.508 ± 0.012	9.5 ± 0.0	5.21 ± 0.07	97.27 ± 6.30	594	5.02	−2.4 ± 3.8	179.8/−31.0/3C 98
5.33.....	0.041 ± 0.003	23.0 ± 0.2	6.82 ± 0.58	134.11 ± 3.95	1016	0.72	4.2 ± 41.4	179.8/−31.0/3C 98
1.48.....	0.092 ± 0.004	−1.0 ± 0.1	4.87 ± 0.22	16.82 ± 5.14	519	0.15	14.7 ± 15.8	179.8/−31.0/3C 98
14.24.....	0.600 ± 0.039	1.4 ± 0.1	2.04 ± 0.08	31.55 ± 2.71	90	0.75	5.2 ± 3.6	39.6/17.1/4C 13.65
10.20.....	0.344 ± 0.023	3.4 ± 0.2	2.57 ± 0.20	35.09 ± 3.09	144	0.60	−8.8 ± 6.5	39.6/17.1/4C 13.65
17.73.....	1.161 ± 0.015	2.0 ± 0.0	2.10 ± 0.02	25.81 ± 6.76	96	1.22	4.7 ± 2.3	43.5/9.2/4C 13.67
18.90.....	1.019 ± 0.010	6.2 ± 0.0	4.01 ± 0.04	29.56 ± 8.37	351	2.36	5.8 ± 3.3	43.5/9.2/4C 13.67
2.36.....	0.030 ± 0.003	20.2 ± 0.4	8.20 ± 0.89	80.73 ± 7.14	1469	0.38	77.6 ± 92.0	43.5/9.2/4C 13.67
67.48.....	4.067 ± 2.174	7.5 ± 0.1	0.90 ± 0.15	68.66 ± 26.77	17	4.90	2.5 ± 10.9	188.1/0.0/4C 22.12
60.36.....	7.911 ± 8.309	4.4 ± 0.1	0.83 ± 0.19	60.38 ± 27.61	14	7.68	8.7 ± 11.3	188.1/0.0/4C 22.12
35.27.....	6.994 ± 1.782	−2.2 ± 0.0	1.26 ± 0.08	35.31 ± 16.92	34	6.05	7.0 ± 4.5	188.1/0.0/4C 22.12
19.49.....	0.840 ± 0.034	15.8 ± 0.1	3.97 ± 0.16	34.28 ± 12.06	345	2.23	25.3 ± 11.0	188.1/0.0/4C 22.12
68.21.....	1.756 ± 0.045	5.1 ± 0.1	11.63 ± 0.21	82.46 ± 27.02	2954	32.79	−55.2 ± 13.5	188.1/0.0/4C 22.12
17.87.....	0.166 ± 0.003	9.6 ± 0.0	1.87 ± 0.04	117.02 ± 10.60	76	0.71	−3.1 ± 4.4	186.8/−7.1/P0531+19
17.77.....	0.474 ± 0.003	1.8 ± 0.0	2.09 ± 0.02	47.10 ± 16.58	95	0.91	0.3 ± 1.9	186.8/−7.1/P0531+19
39.01.....	0.229 ± 0.001	5.5 ± 0.0	8.74 ± 0.06	190.74 ± 13.06	1670	7.43	15.6 ± 7.1	186.8/−7.1/P0531+19
2.81.....	0.073 ± 0.001	−3.6 ± 0.0	2.23 ± 0.02	40.00 ± 1.10	108	0.13	−29.5 ± 19.8	222.5/63.1/P1055+20
16.34.....	1.285 ± 0.042	33.9 ± 0.0	1.70 ± 0.05	22.59 ± 10.30	63	0.96	−0.8 ± 2.1	201.5/0.5/T0629+10
14.47.....	0.271 ± 0.016	30.9 ± 0.1	2.82 ± 0.26	60.90 ± 13.83	173	0.91	31.2 ± 8.8	201.5/0.5/T0629+10
13.92.....	0.354 ± 0.017	23.3 ± 0.1	3.03 ± 0.16	46.68 ± 19.93	201	0.98	−2.8 ± 7.1	201.5/0.5/T0629+10
28.44.....	1.605 ± 0.035	4.9 ± 0.0	4.37 ± 0.06	35.60 ± 14.16	416	4.86	−16.9 ± 3.0	201.5/0.5/T0629+10
46.16.....	0.297 ± 0.005	16.9 ± 0.3	28.09 ± 0.46	179.87 ± 8.78	17249	29.19	45.1 ± 24.0	201.5/0.5/T0629+10
3.96.....	0.152 ± 0.017	−11.9 ± 0.1	1.29 ± 0.16	28.13 ± 7.36	36	0.11	4.0 ± 7.7	201.5/0.5/T0629+10
71.60.....	0.346 ± 0.003	5.2 ± 0.0	10.91 ± 0.06	245.06 ± 4.27	2602	18.00	2.1 ± 3.3	184.6/−5.8/Tau A
8.37.....	1.242 ± 0.007	10.7 ± 0.0	2.09 ± 0.01	11.77 ± 1.06	95	0.59	−3.1 ± 0.6	184.6/−5.8/Tau A

TABLE 1—*Continued*

T_B	τ	V_{LSR}	ΔV	T_s	T_{kmax}	$N(\text{H I})_{20}$	$B_{\parallel}$	(l/b/Source)
2.38.....	0.355 ± 0.008	5.1 ± 0.0	1.79 ± 0.04	7.98 ± 4.20	69	0.10	7.2 ± 1.7	184.6/−5.8/Tau A
18.01.....	0.507 ± 0.005	2.8 ± 0.0	2.61 ± 0.05	45.33 ± 2.88	148	1.17	2.1 ± 1.4	184.6/−5.8/Tau A
0.00.....	2.634 ± 0.105	−48.0 ± 0.0	4.22 ± 0.08	0.00 ± 0.00	388	0.00	9.3 ± 0.5	111.8/−2.1/Cas A
0.00.....	1.598 ± 0.040	−38.0 ± 0.0	6.67 ± 0.11	0.00 ± 0.00	971	0.00	25.0 ± 0.8	111.8/−2.1/Cas A
16.86.....	1.299 ± 0.047	−0.7 ± 0.0	2.89 ± 0.07	23.19 ± 1.63	183	1.70	−0.3 ± 0.6	111.8/−2.1/Cas A

NOTES.—The ordering is by source name as follows: 3C, 4C, P, T, Tau A, Cas A. Temperatures are in K, velocities in km s^{-1}, column densities in 10^{20} cm^{-2}, and magnetic fields in μG. Table 1 is also available in machine-readable form in the electronic edition of the *Astrophysical Journal Supplement*.

reason not to expect $\Delta B_{\parallel}$ to be Gaussian distributed. This allows us to use standard statistical techniques to explore the distribution of field strength and its correlation with other physical parameters beyond the small-number statistics of secure detections.

9.3. *A Good Statistical Sample of Tabular Results*

In a later paper we will perform the detailed statistical analyses on our results. In preparation for this work, here we apply additional criteria to discard an additional selected group of Gaussian components. We discard these for two reasons. One is to avoid cluttering plots. The other is because for some components the errors $\Delta B_{\parallel}$ are likely to depart from the Gaussian distribution; this can happen in profiles affected by component blending, especially when they are noisy.

We discard Zeeman-splitting detections that satisfy any one of the following criteria:

1. The uncertainty $\Delta B_{\parallel} > 10$ μG, unless $|B_{\parallel}|/\Delta B_{\parallel} > 2.5$. We regard such points as outliers because it is highly unlikely for such strong fields to exist in H I clouds.
2. The interpretation of the profile is complicated. This occurs for some low-latitude profiles. The discarded data include 3C 154, 3C 167, 4C 22.12, and T0629+10.
3. The result is suspicious. This is a subjective judgment based on the combination of signal/noise, profile complexity, and the presence of other blended strong components in the same profile that might have reliable detections. These cases, in which our subjective judgment creates criteria, include the following: 3C 192; 3C 274.1; the 18 and 25 km s^{-1} components of 3C 410; the −7, 4, and 11 km s^{-1} components of 3C 78; and P0531+19.

This leaves us with a total of 69 statistically usable components. In Table 1, the magnetic fields of the usable components are in boldface.

9.4. *Comparison with Previous Literature*

To our knowledge, there exist two sources in our list that have previous published detections of H I Zeeman splitting. These are the original discovery of H I Zeeman splitting by Verschuur (1969), who observed both Tau A and Cas A; and the interferometric study of Schwarz et al. (1986), who studied Cas A. The signs of the Cas A Stokes V spectra disagree in these two references. From

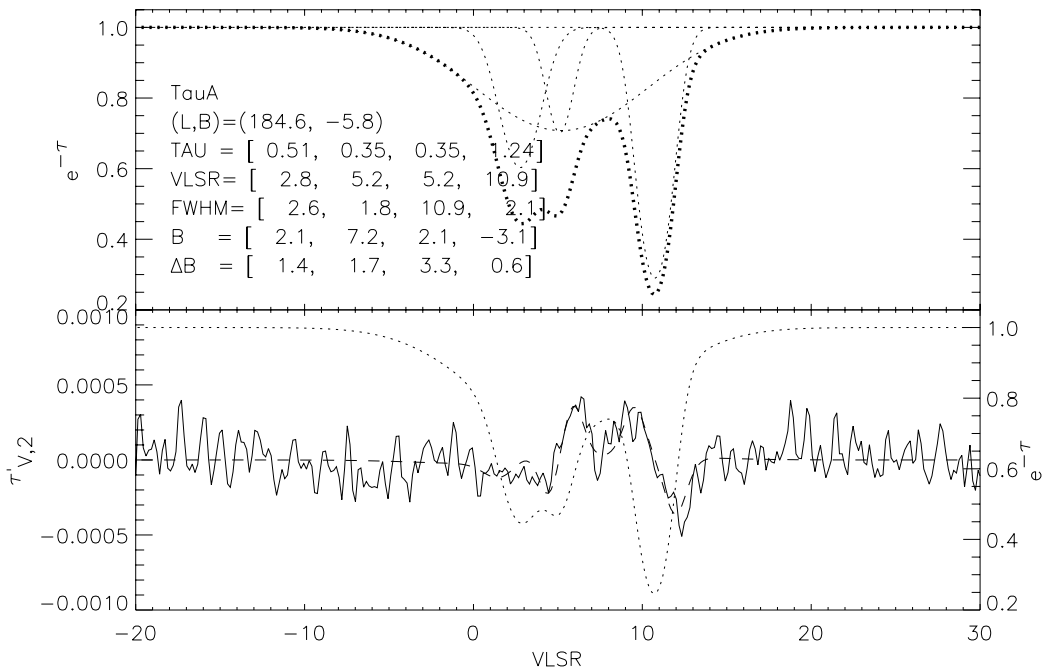

FIG. 10.—Derived spectra for Tau A; the layout of this figure is identical to that of Fig. 9, except that here we omit the bottom panel because Tau A is so strong.

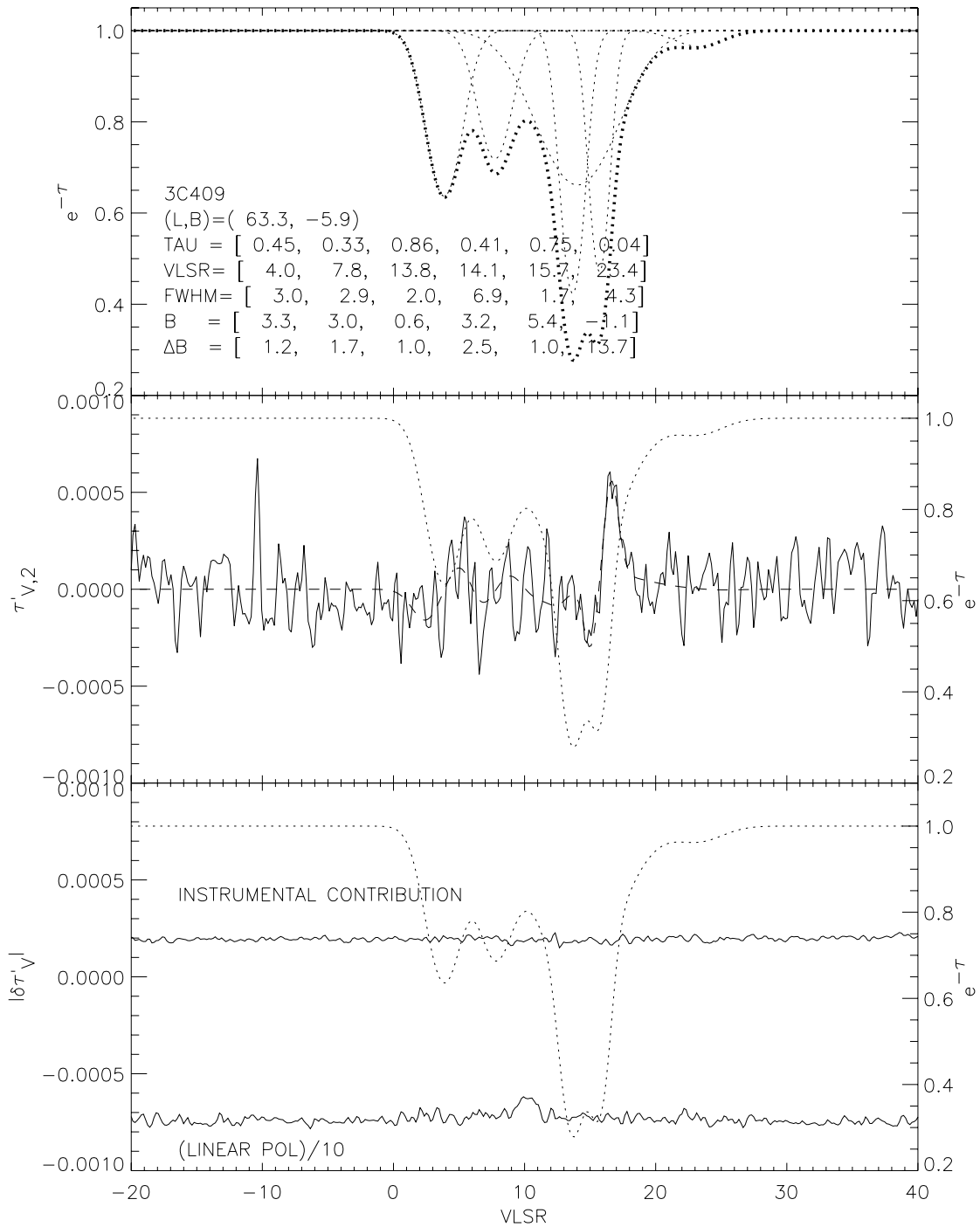

FIG. 11.—Derived spectra for 3C 409; the layout of this figure is identical to that of Fig. 9

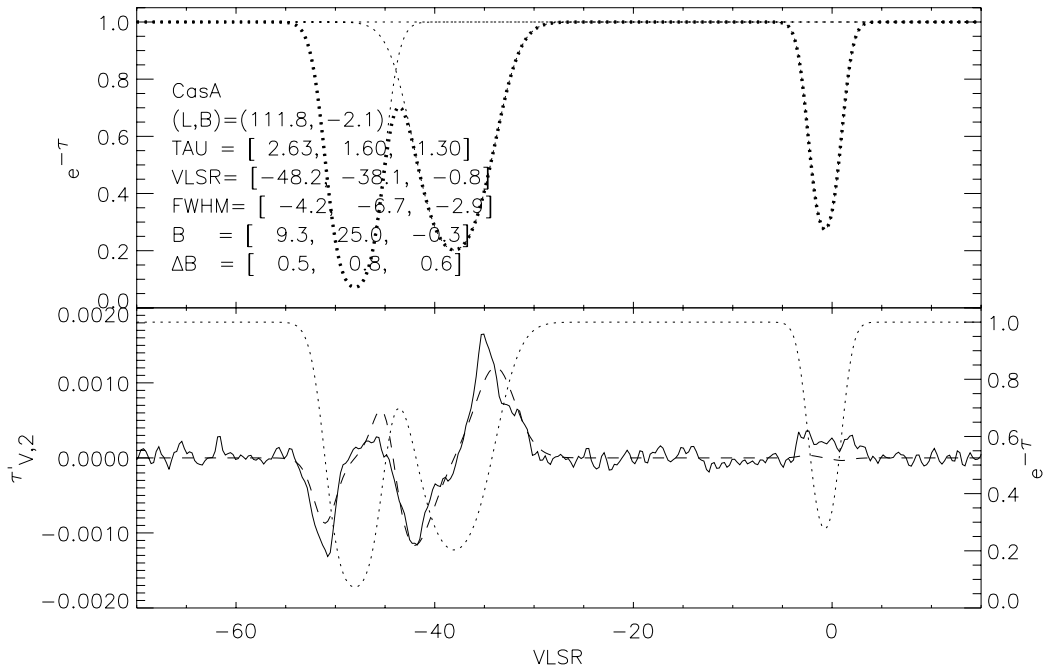

FIG. 12.—Derived spectra for Cas A; the layout of this figure is identical to that of Fig. 9, except that here we omit the bottom panel because Cas A is so strong.

observations of a calibration helix as well as the 1665 MHz OH maser source W49, we have determined that Schwarz et al. (1986) are correct. Verschuur stated that his Stokes V was IEEE LHC–RHC, but this appears to be nothing more than a typographical error. It is not a fundamental sign error because the signs of his derived $B_{\|}$ are correct. Accounting for this typographical error, the previous two references and the current work all agree for Cas A, and we agree with Verschuur for Tau A.

9.5. *Yet Another Source of Uncertainty in $B_{\|}$*

In § 3 of Paper I, we considered the effect of ordering the absorbing clouds along the line of sight. This affects the derived spin temperatures. It also can affect the derived magnetic fields, because the Stokes V spectrum from a background cloud is weakened by a foreground one if the velocity profiles overlap.

This affects the derived $B_{\|}$ only if there is velocity overlap and if the opacities are high. For all of our sources, the fits for the different orderings are visually identical and their variances differ by insignificant amounts. Thus, as in Paper I, we cannot determine the line-of-sight ordering. Nevertheless, the ordering affects the derived magnetic field strengths, as it also does with the spin temperatures in Paper I. For most sources the differences are smaller than the 1 σ uncertainty $\Delta B_{\|}$. For three sources, having a total of four Gaussian components, the differences are larger. All three sources are at low Galactic latitude where blending is a problem. We show the spectra for Tau A, 3C 409, and Cas A in Figures 10, 11, and 12, respectively (the Cas A data are from the Hat Creek 85 foot telescope and are previously unpublished).

Table 2 lists the four components for which $B_{\|}$ is affected by more than the 1 σ error $\Delta B_{\|}$. We list three values of field. $B_{\|,0}$ is the value from Table 1; $B_{\|,\max}$ and $B_{\|,\min}$ are the minimum and maximum values obtained from permuting the line-of-sight orderings. These differences exceed $\Delta B_{\|}$ but are nevertheless modest fractions of the derived $B_{\|}$. Consequently, we ignore this extra source of uncertainty both in Table 1 and in our future analyses.

TABLE 2
DEPENDENCE OF $B_{\|}$ ON CLOUD ORDERING

Source/VLSR	$B_{\|,0}$	$B_{\|,\max}$	$B_{\|,\min}$
Tau A/10.7	−3.09 ± 0.55	−3.66 ± 0.65	−3.09 ± 0.55
Tau A/5.1	7.19 ± 1.69	10.56 ± 2.50	7.10 ± 1.67
3C 409/15.7	5.74 ± 1.06	8.03 ± 1.47	5.74 ± 1.01
Cas A/−48.0	9.29 ± 0.54	9.74 ± 0.55	8.70 ± 0.55

NOTES.—$B_{\|,0}$ is from Table 1; $B_{\|,\max}$ and $B_{\|,\min}$ are the largest and smallest fields derived including opacity effects (see § 9.5). Magnetic fields are in μG and VLSR in km s^{-1}.

10. SUMMARY

We discuss the measurement of polarized Stokes parameter profiles (Q, U, V) from emission/absorption line observations toward background continuum sources. For each of these Stokes parameters, we derive the *opacity profile* and the *emission profile* expected if the continuum source were absent. We give special emphasis to the evaluation of instrumental effects. A principal motivation for our study is detection of the Zeeman effect in Stokes V profiles. Arecibo suffers with respect to other telescopes because its large central blockage produces large sidelobes. The sidelobes are polarized, and their interaction with spatially extended 21 cm emission produces most of the instrumental contributions to the polarized profiles. These contributions are particularly serious for emission profiles. But Arecibo's large collecting area compensates for this problem when measuring opacity profiles. As a result, our Stokes V opacity profiles are generally reliable, so we can make 21 cm Zeeman effect measurements in the Galactic CNM.

In § 2 we outline the basic theoretical concepts involving Stokes parameters in emission/absorption line observations. Here we derive the fundamental equations (5a)–(5b). This equation relates the *observed* Stokes parameter profiles (on- and off-source) to the physically significant polarized opacity profiles and polarized emission profiles. In § 2 we also explain the contribution of the Zeeman effect to the Stokes V profiles. This contribution is always proportional to the derivative of the Stokes I profile (emission or absorption), regardless of the line opacity. Therefore, we can always derive line-of-sight magnetic fields by fitting the Stokes V profile to the derivative of the Stokes I profile.

In § 3 we present equations (10a)–(10d). These are the fundamental equations that we least-squares fit (independently for each spectral channel) to derive the Stokes V opacity profile and the Stokes V emission profile for each source. These equations include an instrumental error term that is extensively discussed in later sections. In § 3 we also present the related discussion for Stokes Q, U profiles, including equation (12). This equation, the analog of equations (10a)–(10d) for Stokes V, includes a rotation matrix to account for the parallactic angles of the observations.

Much of the paper is concerned with instrumental effects arising from polarized beam structure. This structure interacts with spatially extended line emission. As a result, instrumental effects appear in the polarized emission profiles and, to a much smaller extent, in the polarized opacity profiles. In § 4 we describe the nature and the effects of various types of polarized beam structure. One type is "beam squint." Beam squint interacts with the first spatial derivative of the Stokes I profile to make instrumental contributions to the Stokes Q, U, V profiles. Unfortunately, the beam squint contribution to the Stokes V profiles can mimic the Zeeman effect. If beam squint remains fixed relative to the telescope feed system, then its contributions to the polarized Stokes profiles vary with the parallactic angle PA. Another type of polarized beam structure is "beam squash." Beam squash interacts with the *second* derivatives of the Stokes I profile to make instrumental contributions to Stokes Q, U, V. If beam squash remains fixed relative to the telescope feed system, then its contributions vary as 2 PA. For prime focus telescopes, beam squint is theoretically expected only for Stokes V, and beam squash is expected only for Stokes Q, U. However, Arecibo breaks these rules, having beam squint and squash in all polarized Stokes parameters. The final type of polarized beam structure arises outside the primary beam and first sidelobe, in the "far-out sidelobes." Far-out sidelobes at Arecibo are particularly strong because of the large aperture blockage. We define all contributions to the polarized Stokes profiles as "squintlike" and "squashlike" if they are functions of PA and 2PA, respectively. In practice, squintlike contributions may arise from true beam squint (in the primary beam and nearest sidelobe) and, also, from the far-out sidelobes. The same is true for beam squash.

In § 5 we treat instrumental squintlike and squashlike contributions to Stokes V opacity profiles. These profiles are of particular interest for the Zeeman effect. Equations (13a)–(13b) express these instrumental contributions to the fundamental fitting equation (eqs. [10a]–[10d]) as sinusoidal functions of PA (squintlike) and 2PA (squashlike). We fit equations (10a)–(10d) in three ways: (a) with neither squintlike nor squashlike contributions included, (b) with squintlike contributions only, and (c) with both squintlike and squashlike contributions. Results of these three types of fits are Stokes V opacity profiles and emission profiles with (a) no instrumental effects removed, (b) squintlike effects removed, and (c) both squintlike and squashlike effects removed, respectively. Fits of type (c) are usually best for the Stokes V opacity profiles, allowing us to remove squintlike and squashlike contributions accurately. In § 5.2, we illustrate these concepts for 3C 138, which has a clearly detected Zeeman effect. In this section, we also develop a matrix representation of the coupling coefficients between the fitted Stokes V opacity profile for a given source and the squintlike and squashlike instrumental contributions. From this matrix, we derive a profile of $\delta\tau'_{V,2}(\nu)$ for each source. This profile represents the maximum possible instrumental contributions to the Stokes V opacity profile after squintlike and squashlike contributions have been removed by the fitting process. An example for 3C 138 is shown in the bottom panel of Figure 9*a*. Here the profile of $\delta\tau'_{V,2}(\nu)$ is insignificant compared to the Zeeman effect in the Stokes V opacity profile. For most sources, the profile $\delta\tau'_{V,2}(\nu)$ is very small compared to that of the Stokes V opacity profile, another reason to expect that the latter are reliably determined.

Section 6 treats squintlike and squashlike contributions to the linear polarization Stokes Q, U opacity profiles. Least-squares fits for squashlike contributions are not possible: squashlike effects have the same 2 PA dependence as true linear polarization, so the two cannot be distinguished. However, true linear polarization of the H I opacity profile should be very small, particularly for small sources like 3C 454.3 (angular size 14 milliarcsec). Therefore, the apparent linear polarization we measure in the 3C 454.3 opacity profile must be instrumental. We judge that the same conclusion holds for all sources, leading to a second method of estimating instrumental effects in Stokes V opacity profiles. The Arecibo beam squint and squash are known to be about 10 times greater in Stokes Q, U than in Stokes V. Therefore, we can estimate instrumental polarization in Stokes V opacity profiles by dividing the apparent linear polarization in the Stokes Q, U profiles by 10. Since squintlike and squashlike effects have already been removed from Stokes V opacity profiles, this estimate applies to instrumental effects (including those from the far-out sidelobes) that are not a function of PA or 2 PA. This technique is described in § 7, and an illustrative profile for 3C 138 is shown in the bottom panel of Figure 9*a*.

Our final discussion of instrumental effects (§ 8) addresses the reliability of the Stokes V emission profiles. For these profiles, fits of type (c) usually suffer from large covariance between the PA and 2PA-dependent fit parameters. As a result, the fit parameters are poorly determined, and the type (c) fits yield very noisy Stokes V emission profiles. An example for 3C 138 is shown in the bottom panel of Figure 5. In effect, we are unable to remove reliably the squintlike and squashlike contributions from the Stokes V emission profiles so we cannot derive the Zeeman effect from them. Covariance between the fit parameters would be much less if we had a larger range of PA included in the data sets for our sources. In § 8 we also independently evaluate the contributions of *true* beam squint and squash (from the main beam and the first sidelobe) to the Stokes V emission profiles. We compare these contributions to the empirically fitted squintlike and squashlike contributions (from the main beam and all sidelobes). The difference between these two is the contribution from the far-out sidelobes alone. We find that the far-out sidelobes contribute most of the instrumental effects at Arecibo. We expect these contributions to be mainly squintlike or squashlike, but there might also other contributions that do not depend on PA or 2PA; such contributions contribute additional uncertainties. For all these reasons, Zeeman effect results derived from Arecibo Stokes V emission profiles are unreliable.

Section 9 presents the Stokes I and V opacity profiles for all sources, along with profiles of possible instrumental effects in the latter. Profiles for 3C 138 are shown in Figure 9*a*, profiles for other sources others are provided electronically. This section also presents a tabular list of parameters, including line-of-sight magnetic field strengths, for the CNM Gaussian components in the Stokes I opacity profiles. We select a sample 69 Gaussian components for which $\Delta B_{\|}$ (uncertainties in the derived $B_{\|}$) should be Gaussian distributed and, additionally, for which $\Delta B_{\|} < 10$ μG. We will subject this sample to a future statistical analysis of magnetic field strengths in the CNM. In § 9, we also discuss another source of uncertainty in derived magnetic field strengths, the unknown sequential order along the line of sight of the various CNM velocity components. However, this source of error has no significant effect upon the qualitative or statistical properties of the magnetic field measurements.

This work was supported in part by NSF grants AST-9530590, AST-0097417, and AST-9988341, and by the NAIC.

REFERENCES

Fomalont, E. B., et al. 2000, ApJS, 131, 95
Heiles, C. 1989, ApJ, 336, 808
———. 1996, ApJ, 466, 224
———. 1997, ApJ, 481, 193
———. 2001, PASP, 113, 1243
Heiles, C., & Troland, T. 2003a, ApJS, 145, 329 (Paper I)
Heiles, C., & Troland, T. 2003b, ApJ, 586, 1067 (Paper II)
Heiles, C., et al. 2001a, PASP, 113, 1247
———. 2001b, PASP, 113, 1274
Schwarz, U., Troland, T. H., Albinson, J. S., Bregman, J. D., Goss, W. M., & Heiles, C. 1986, A&A, 118, 157
Verschuur, G. L. 1969, ApJ, 156, 861